

Article

Paleogeographic Evolution of Southeast Asia: Geochemistry and Geochronology of the Katha-Gangaw Range, Northern Myanmar

Myo Myint Aung ^{1,2}, Lin Ding ^{1,2}, Upendra Baral ^{1,3,*}, Fulong Cai ^{1,2}, Bhupati Neupane ^{3,4}, Me Me Aung ⁵, Aung Naing Thu ⁵, Kyaing Sein ⁶ and Kyawt Kay Khaing ⁷

- ¹ State Key Laboratory of Tibetan Plateau Earth System Science, Resources and Environment, Institute of Tibetan Plateau Research, Chinese Academy of Sciences, Beijing 100101, China
 - ² University of Chinese Academy of Sciences, Beijing 101408, China
 - ³ Institute of Fundamental Research and Studies (InFeRS), Kathmandu 44600, Nepal
 - ⁴ Department of Civil Engineering, Sagarmatha Engineering College, Lalitpur 44600, Nepal
 - ⁵ Department of Geology, University of Myitkyina, Myitkyina 01020, Myanmar
 - ⁶ Myanmar Geoscience Society, Yangon 11041, Myanmar
 - ⁷ School of Earth Sciences and Resources, China University of Geosciences, Beijing 100083, China
- * Correspondence: upendrabaral@gmail.com



Citation: Aung, M.M.; Ding, L.; Baral, U.; Cai, F.; Neupane, B.; Aung, M.M.; Thu, A.N.; Sein, K.; Khaing, K.K. Paleogeographic Evolution of Southeast Asia: Geochemistry and Geochronology of the Katha-Gangaw Range, Northern Myanmar. *Minerals* **2022**, *12*, 1632. <https://doi.org/10.3390/min12121632>

Academic Editor: Simon Paul Johnson

Received: 5 October 2022

Accepted: 13 December 2022

Published: 18 December 2022

Publisher's Note: MDPI stays neutral with regard to jurisdictional claims in published maps and institutional affiliations.



Copyright: © 2022 by the authors. Licensee MDPI, Basel, Switzerland. This article is an open access article distributed under the terms and conditions of the Creative Commons Attribution (CC BY) license (<https://creativecommons.org/licenses/by/4.0/>).

Abstract: The Mogok continental foreland region and Katha-Gangaw range (KGR) are located in the north-central section of the Myanmar plate, which is a component of the Eurasian plate. The origin of KGR, exposed along northern Myanmar (SE Asia), is still up for argument, despite numerous prior studies. Based on the petrography, geochemistry, and detrital zircon U-Pb geochronology of metamorphic rock samples, the current study focuses on the tectonic evolution of the KGR. The study also emphasizes the phenomenon of microcontinents rifting from the Gondwanan supercontinent and their subsequent amalgamation with Asia. Detrital zircon ages from four samples in the southern region of KGR peak at 634 Ma, 525 Ma, 290 Ma, and 248 Ma, and two samples yielded > 40% of the grains of younger than 400 Ma. Similar results were obtained from three samples (out of six) from the central region of the KGR. All of the samples from the northern part of KGR are older than 400 Ma, with the exception of MT-02A, which contains nearly all of the younger grains. These younger peaks are identical to the zircon U-Pb ages of the Indochina block, the Sibumasu block, and the Pane Chaung Formation of the Myanmar plate, as well as the Langjiexue Formation (southeastern Tibet). This similarity raises the possibility of either these units being a source region of strata in northern Myanmar or sharing a similar source. The geochemistry of metamorphic rocks samples from KGR revealed loss-on-ignition (LOI) values of 0.29–4.18 wt%, emphasizing the modest to moderate alteration. The samples are enriched in large-ion lithophile elements (LILEs), and depleted in high-field strength elements (HFSEs). All metamorphic samples are peraluminous, indicating the linkage with collisional orogenies. This result is most comparable to upper continental crustal provenance. Hence, the metamorphic rocks in KGR regions must be associated with the crustal materials.

Keywords: India–Asia collision; U-Pb geochronology; geochemistry; Katha-Gangaw Range; Northern Myanmar

1. Introduction

The Myanmar plate is a small tectonic plate situated in Southeast Asia that is part of the larger Eurasian plate, bounded by the Indo-Burma outer wedge to the west and the Sagaing fault, Shan-Thai Plateau and Mogok Metamorphic Belt (MMB; Sibumasu block) to the east. The study of this region can provide insightful information on the evolutionary history of Southeast Asia as well as the accretion of terranes and microcontinents following the Gondwana breakoff [1,2]. The north-central portion of present-day Myanmar comprises

the Mogok continental foreland region and the Katha-Gangaw Range (KGR). The KGR is bounded by the Sagaing fault and MMB in the east and west, respectively (Figure 1a) [3–6]. The Sagaing fault is ~1200 km long right-lateral strike-slip fault that runs most of the length of Myanmar and cuts the western margin of the Mogok belt [7–10]. The Central Myanmar Basin (CMB) is located west of the KGR (Figure 1a,b), and it was developed on the upper plate of the convergent margin between the Myanmar plate and Sibumasu terrane. The Sibumasu terrane is a part of continental crust spreading from Lhasa to Southeast Asia [11]. This CMB records the tectonic, sedimentary, and magmatic processes associated with subduction of oceanic lithosphere [12–14]. More particularly, during the Mesozoic–Cenozoic subduction, several forearc basins were developed adjacent to the Indo-Burman accretionary complex, and it records the deep-water turbidite strata [12].

The accretion history of Southeast Asia has been studied in the past using diverse methodologies, such as geological mapping, geochemistry, geochronology, paleomagnetism, and sedimentology [1,15–19]. The rifting of both Indochina and south China blocks from the eastern Gondwana margin started during the Devonian, resulting in the opening of Paleo–Tethys Ocean [18,20]. Nevertheless, some argue that the Sibumasu terrane was rifted from the eastern Gondwana only during the Early Permian [21,22]. The presence of Ordovician to Lower Jurassic strata within the Sibumasu terrane supports the Devonian rifting [1,23]. After this rifting event, a peripheral foreland basin was developed in central Myanmar during the Eocene in which clastic sedimentary rocks were deposited and those sediments were primarily sourced from the erosional unroofing of a Cretaceous–Eocene Andean-type magmatic arc [24]. This magmatic arc was formed prior to and after the India–Asia collision [24] and related to the subduction of Neo-Tethys oceanic slab beneath the Asian continental margin [25,26]. This hypothesis is supported by the presence of a calc-alkaline andesitic volcanic arc (ca. 101–43 Ma), presently found in the northeast of the CMB.

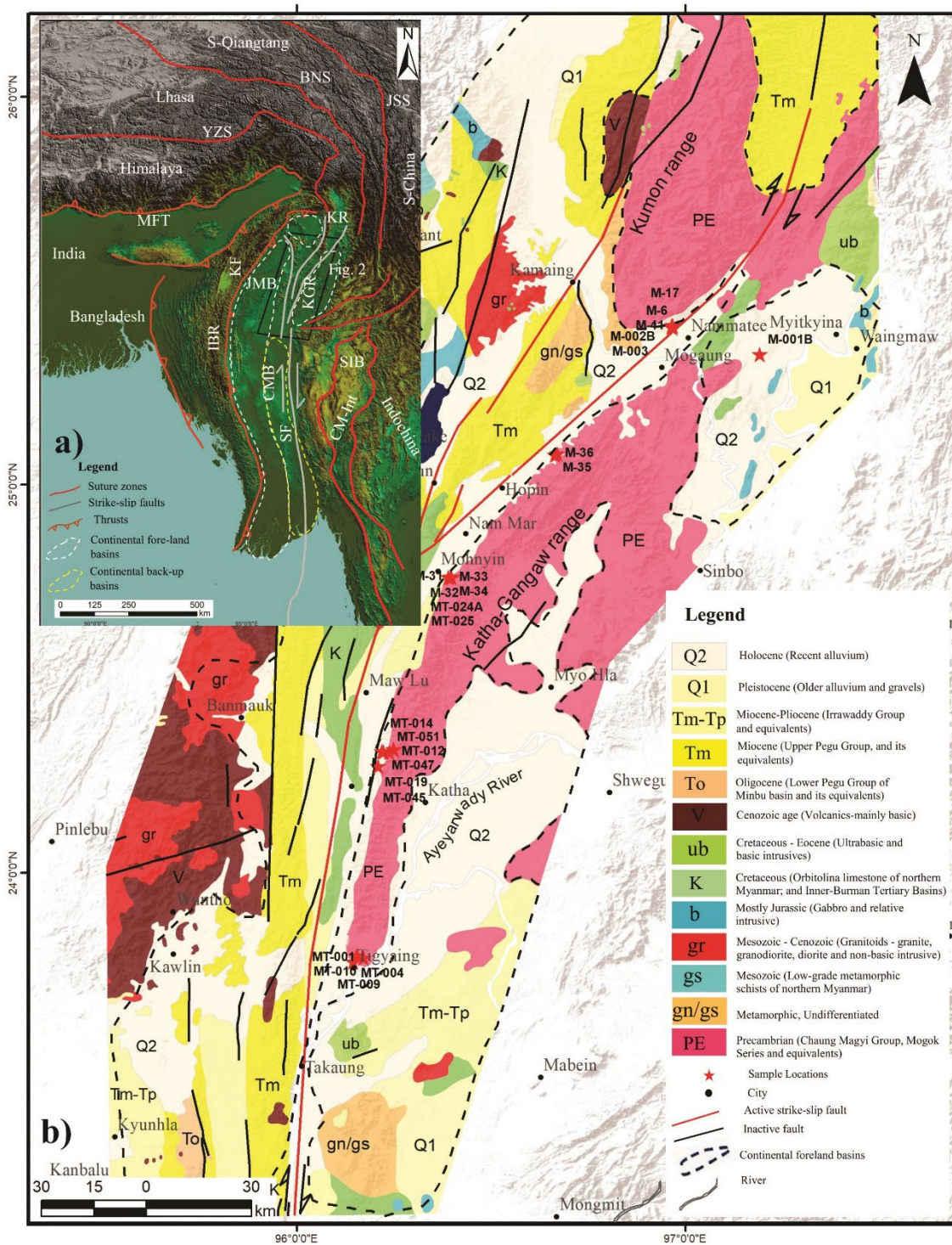


Figure 1. (a) Simplified geological map of India–Asia collision zone including present-day Myanmar [3,4,23,27]. CB = Central Burma, SF = Sagaing Fault, IBR = Indo-Burmar Ranges, JMB = Jade Mine Belt, KGR = Katha- Gangaw Range, KR = Kumon Range, KF = Kabaw Fault, MFT = Main Front Thrust, YZS = Yarlung Zangbo Suture Zone, BNS = Bangong-Nujiang Suture Zone, JSS = Jinsha suture zone, CM-Int = Changning–Menglian and Inthanon suture zones, SIB = Sibumasu. **(b)** Generalized geological map including the Katha-Gangaw range and the southernmost part of the Kumon range. The rectangular box in (a) marks the boundary of (b).

Recently, some studies have constrained two unconformities: Late Eocene–Middle Oligocene and the latest Oligocene–Early Miocene ages, which are linked with the north-

ward translation of the Myanmar plate with the Asian margin [28]. These studies stated that the fluvial environment, with the occurrence of reworked sediments at the first unconformity, likely recorded the commencement of the collision of the Indian plate and the northern extent of the Myanmar plate with the Asian plate. The second unconformity showed a drastic change in magnetic properties, mineralogy, and provenance, along with high-grade metamorphic minerals. Hence, both of these unconformities suggest the indentation of the Myanmar plate into the eastern Himalayan collision zone, resulting the modern eastern Himalayan Syntaxes. According to Metcalfe [29], the western Myanmar block was rifted from Gondwana in the Devonian, then from Late Permian to Early Triassic, it accreted to the Sibumasu terrane. Later, it slipped westward along the boundary fault [30], resulting in the modern western Myanmar block. In the Eocene, the western Myanmar block transitioned from a passive to an active continental margin [31].

However, despite several studies having been conducted, a constructive model of regional tectonic evolution for northern Myanmar has still not been presented [32–34]. Similarly, paleogeographic correlations and collision age estimates remain a subject of debate. To address this issue, the present study conducted petrographic analyses and U-Pb detrital zircon geochronology (17 samples) of metamorphic rocks from the southernmost Kumon and Katha-Gangaw ranges. In addition, the study also conducted geochemical analyses of metamorphic rocks (eight samples) from the same area. The present study findings, along with published data, suggest that the rocks exposed along the KGR were deposited adjacent to the northern margin of Australia, and were mostly sourced from Gondwana and/or the Tethys Himalaya. In addition, the detrital zircon age spectra do not include ages indicative of Sibumasu terrane, further highlighting that Sibumasu and the Indochina block did not collide until the Early Triassic to Permian.

2. Regional Geology and Tectonic Background

The India plate collided with northern Myanmar and Tibet along a suture in the latest Eocene, following repeated northward and eastward subduction of the Tethyan ocean (Figure 1b) [35]. During the Cenozoic, the Burma terrane (Myanmar plate) traveled about 2000 km northward to the Indian plate before colliding with the Asian margin. This activity played a key role in the paleogeographic evolution of the Burma terrane and the eastern Himalayan orogen [28]. The present-day Myanmar region (Burma terrane) is divided into four major lithostratigraphic units: the Indo-Burma range (IBR), also known as the Indo-Burman Wedge (IBW), CMB, MMB, and the Shan Plateau, from the west to east [1,35–38].

The metamorphic rocks of KGR trending in an NNE–SSW direction, and more especially in the Tigyain–Katha–Indaw area, are divided into three informal units. Unit I, mainly composed of garnet–biotite schist, garnet–graphite schist, garnet–staurolite schist, garnet quartzite, quartz–mica schist, garnet–hornblende schist, and garnet–barroisite schist. Biotite schist, micaceous quartzite, chloritoid schist, and actinolite schist represent Unit II, and Unit III contains chlorite phyllite, chlorite schist, graphite schist, and quartzite [39].

The Shan Plateau (Shan–Thai block) rifted from Gondwana during the Early Permian [40] and collided with Asia in the Early Triassic [22] or Late Triassic [41,42]. It consists of Upper Cambrian to Devonian and mid-Permian to Early Mesozoic geologic succession [43]. In addition, the Shan Plateau consists of Paleozoic–Mesozoic limestone, dolomite, and clastic sedimentary rocks [44]. This plateau structurally overlays the Jurassic and mid-Cretaceous metamorphic rocks (ca. 40–30 Ma; suggesting recent metamorphic events in the Late Eocene–Oligocene) of the Chaung Magyi Group [45].

The MMB is located on the western margin of the Shan Plateau [4] and extends to the western Malaysia and eastern Sumatra [42]. This MMB was rifted from Gondwana [40] and collided with the Eurasia either in the Late Jurassic [41,42] or Early Triassic [22]. It consists of marbles, gneisses, migmatites, garnet schists, mica schists, rare quartzites, and granulite facies rocks along with some intrusive materials like granites [37,46]. Mogok metamorphic protolith ages range from 491 Ma to 114 Ma, with a number of metamorphism

events at 128 Ma, 43–29 Ma, and 26–21 Ma [37,46]. The MMB experienced two major metamorphic events at ~128 Ma and ~47–29 Ma [46] that involved the intrusion of the Cretaceous–Paleogene (K/Pg) granitoids and pegmatites [37,46,47]. The eastern part of the MMB consists of kyanite schists and quartzites, and lower-grade mica, chlorite, and talc schists to the east.

The CMB is a 25 m thick succession of Upper Cretaceous to Cenozoic sedimentary rocks deposited in fluvio-deltaic systems that prograded southwards across a shallow marine depositional setting [38,44,48]. The CMB is further divided into the eastern and western segments by the Central Volcanic Line and Sagaing fault [38,44,49,50]. In western Myanmar, the CMB is interpreted as an accretionary prism, including slivers of a dismembered ophiolite, obducted above the east-dipping subduction zone [44,51,52]. The CMB contains five back-arc and four fore-arc basins in the eastern and western parts, respectively [27,48]. These sub-basins were the result of Myanmar–Eurasia collision [38,44,48] and are mostly located on the continental margin [35,52,53]. Notably, during the Miocene, the Myanmar plate acted as a forearc sliver coupled with the Indian plate and moved northward relative to the Asian plate along the Sagaing fault. The Sagaing fault is a plate boundary that separates the Myanmar plate from Southeast Asia [51,54]. Near the Sagaing fault, geomorphic characteristics and earthquake focal-mechanism solutions reveal right-lateral slip [54]. It is suggested that since the Late Cretaceous, the Myanmar plate has migrated over 1000 km north of Southeast Asia [35].

The western part of Myanmar is occupied by the IBR, which is an active west-verging accretionary complex that propagated in the Bengal basin [44]. The IBR consists of two units: (i) Yarlung–Tsangpo Suture zone of Cretaceous ophiolitic rocks [55], and (ii) Upper Triassic Pane Chaung Formation and Kanpetlet schist [56,57]. The IBR also consists of the longest ophiolite belt, which extends from the eastern Naga Hills to the Rakhine ranges and comprises ultramafic rocks, mafic dykes, pillow lava, spilite, radiolarian chert, and flysch-type sedimentary rocks [58,59]. Furthermore, the Cretaceous sequences of the IBR are composed of mudstone, turbiditic sediments, and limestone containing Late Cretaceous foraminifera [7,44]. The overlying Paleocene strata consist of mudstone, limestone, and minor sandstone.

3. Methodology

The metamorphic samples were collected from the KGR, specifically from the splayed zone of the Sagaing fault in northern Myanmar (Figure 1b, Table 1). Petrographic studies, cathodoluminescence imaging (CL), U-Pb detrital zircon geochronology and whole rock geochemistry analyses were conducted at the State Key Laboratory of Tibetan Plateau Earth System Science, Resources and Environment, Institute of Tibetan Plateau Research, Chinese Academy of Sciences, Beijing. Whole-rock major element analysis was carried out at the Institute of Geology and Geophysics, Chinese Academy of Sciences (IGG-CAS), Beijing.

Table 1. Sample lithology, locations, and depositional ages from this study. Abbreviations: K-G Range (S) = southernmost part of Katha-Gangaw range; K-G Range (L-M) = Lower middle part of Katha-Gangaw range; K-G Range (U-M) = Upper middle part of Katha-Gangaw range; K-G Range (N) = Northernmost part of Katha-Gangaw range; Kumon range (S) = southernmost part of Kumon Range; Gnt-Stauroilite Schist = Garnet–Stauroilite Schist.

Samples	Area	Rock Type	Age	Latitude (N)	Longitude (E)
MT-001	KGR (S)	Quartzite	Cambrian–Proterozoic	23°46′49.98″ N	96°10′17.84″ E
MT-004	KGR (S)	Quartzite	Cambrian–Proterozoic	23°46′14.36″ N	96°08′40.98″ E
MT-009	KGR (S)	Quartzite	Mesozoic–Proterozoic	23°47′10.23″ N	96°09′19.18″ E

Table 1. Cont.

Samples	Area	Rock Type	Age	Latitude (N)	Longitude (E)
MT-010	KGR (S)	Quartzite	Mesozoic–Proterozoic	23°47′10.23″ N	96°09′19.18″ E
MT-012	KGR (L-M)	Quartzite	Mesozoic–Proterozoic	24°18′48.47″ N	96°13′10.53″ E
MT-014	KGR (L-M)	Quartzite	Cambrian–Proterozoic	24°18′44.59″ N	96°13′24.01″ E
MT-019	KGR (L-M)	Quartzite	Cambrian–Proterozoic	24°16′26.59″ N	96°12′34.58″ E
MT-024A	KGR (U-M)	Quartzite	Cambrian–Proterozoic	24°45′40.73″ N	96°23′52.33″ E
MT-025	KGR (U-M)	Quartzite	Cambrian–Proterozoic	24°45′41.49″ N	96°23′54.19″ E
MT-045	KGR (L-M)	Quartzite	Mesozoic–Proterozoic	24°19′05.82″ N	96°14′59.20″ E
MT-047	KGR (L-M)	Quartzite	Mesozoic	24°19′04.20″ N	96°14′58.11″ E
MT-051	KGR (L-M)	Quartzite	Cambrian–Proterozoic	24°18′40.17″ N	96°14′16.10″ E
M-31	KGR (U-M)	Quartzite	Cambrian–Proterozoic	24°45′43.24″ N	96°23′52.12″ E
M-32	KGR (U-M)	Quartzite	Cambrian–Proterozoic	24°45′43.24″ N	96°23′52.12″ E
M-34	KGR (U-M)	Quartzite	Cambrian–Proterozoic	24°45′42.94″ N	96°23′52.40″ E
M-6	KR	Mylonite gneiss	Proterozoic	25°24′34.82″ N	96°58′05.33″ E
M-002A	KR	Mylonite gneiss	Proterozoic	25°24′29.88″ N	96°57′55.25″ E
M-003	KR (S)	Mylonite gneiss	Proterozoic	25°24′27.55″ N	96°57′54.59″ E
M-17	KR (S)	Mica-Schist	Proterozoic	25°24′41.36″ N	96°58′03.22″ E
M-41	KR (S)	Biotite-Gneiss	Proterozoic	25°24′14.82″ N	96°58′03.71″ E
M-33	KGR (N)	Gnt-Kyanite Schist	Cenozoic–Mesozoic	24°45′42.94″ N	96°23′52.40″ E
M-35	KGR (N)	Gnt-Staurolite Schist	Cambrian–Proterozoic	25°04′38.46″ N	96°39′51.81″ E
M-36	KGR (N)	Gnt-Staurolite Schist	Cambrian–Proterozoic	25°04′47.62″ N	96°40′13.59″ E

3.1. Detrital Zircon U-Pb Dating Method

Four samples (MT-001, MT-004, MT-009, and MT-010) from the southern part of KGR in the Tigyain area (Figure 2a,b), and six samples (MT-012, MT-014, MT-019, MT-045, MT-047, and MT-051) from the middle part of KGR in the Katha-Indaw area (Figure 2c,d) were analyzed. Similarly, seven samples (MT-024A, MT-025, M-31, M-32, M-34, M-35, and M-36) from the northern part of KGR in the east of Mohgyin and Pinbaw areas (Figure 2e,f) were further examined.

Detrital zircons were extracted from ~3–5 kg rock samples using conventional heavy liquid and magnetic separation techniques [37,60]. The zircon grains were handpicked, mounted in epoxy resin, and polished to obtain an unweathered surface. The CL images were used to determine the zircon morphology and unweathered grains were analyzed via laser ablation multi-collector inductively coupled plasma mass spectrometry (LA-MC-ICP MS) manufactured in CA, USA attached with Agilent 7500a New Wave Research Instruments UP193FX Excimer Laser manufactured in CA, USA. Spot sizes ranging from 25 µm to 35 µm were used for the analysis. The ions generated by laser ablation with a 25 to 35 µm spot diameter, a 7 Hz repetition rate, and 5–8 J/cm² energy were transported via high-purity helium and argon gas. The flow of carrier gases was tuned following the ablation of standard NIST 610 to produce the strongest signal possible for ²³⁸U and ²⁰⁸Pb. At the same time, it reduced oxide interference and generated the most consistent signal intensity. Individual analytical runtimes were about 100 s (15 s for acquiring blank data, 40 s for acquiring data from samples that had been abated, and 45 s for the washout period). The detailed procedure is available in Cai, Ding and Yue [32]. The NIST 610 sample and ²⁹Si were used

as external and internal standards, respectively. The raw count rates for ^{29}Si , ^{204}Pb , ^{206}Pb , ^{207}Pb , ^{208}Pb , ^{232}Th , and ^{238}U were recorded. For age interpretation, $^{206}\text{Pb}/^{238}\text{U}$ ages and $^{206}\text{Pb}/^{207}\text{Pb}$ ages were used for grains with ages < 1000 Ma and > 1000 Ma, respectively. Ages with an uncertainty $> 10\%$ ($^{206}\text{Pb}/^{238}\text{U}$), discordance $> 20\%$ or reverse discordance $> 5\%$ were excluded from the interpretation. The $U\text{-Pb}$ ages were calculated using GLITTER 4.0, which was calibrated using zircon standard Plesovice (337 ± 0.37 Ma; [24,61]). The results were plotted using Isoplot 3.7. A common lead correction and detailed age plot procedure was performed following Andersen [62] and Cai, Ding and Yue [32]. The geochronology results are illustrated in Table S1.

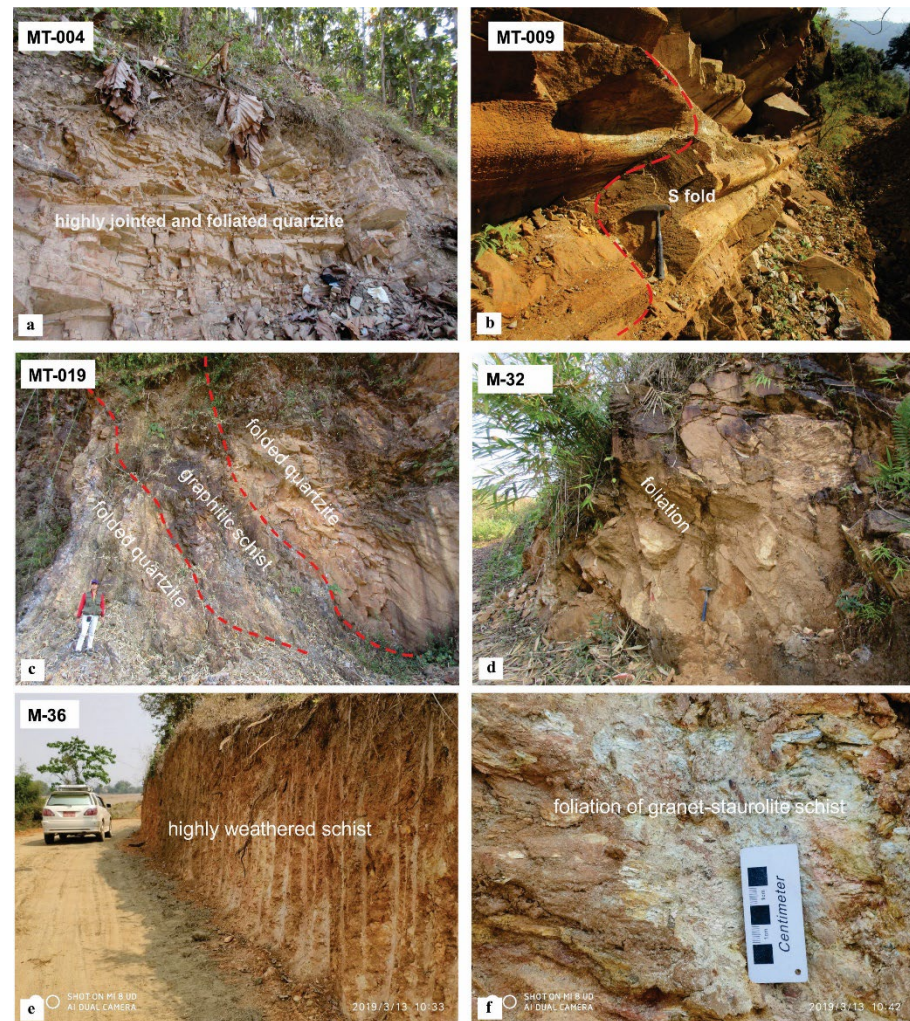


Figure 2. Selected quartzite sample outcrops within the Katha-Gangaw range Mesozoic to Cenozoic period. (a) Highly jointed micaceous quartzites in the Tigyaing-Katha area, (b) quartzite S-fold trending 195/52, located northeast of Nabar, (c) graphite schists are intercalated between thick bedded and folded quartzite located at the south-middle part of the Katha-Gangaw range, and the red lines show the foliation trace of quartzite and graphite schist. (d) Quartzite exposed east of Mohgyin area, and (e,f) garnet–staurolite schist exposed east of the Pinbaw area in the northern part of the Katha-Gangaw range with their foliation structures.

In this study, the maximum depositional age (MDA) was determined by the weighted average of the youngest two or more grains that overlapped in age, with a 1σ standard deviation [63]. The MDA algorithm's main goal is to determine the upper limit of the depositional age. Although it makes no difference if this upper limit is related to a single geological event or a collection of numerous overlapping occurrences [64], it is worth

mentioning that even if several of the youngest ages were dispersive (i.e., did not overlap in age at 1σ), the MDA was much older than the actual depositional age. Thus, as a less-than-ideal alternative, the youngest single age was used to roughly constrain the maximum depositional age.

3.2. Whole—Rock Geochemistry

Eight metamorphic rock samples (M-002A, M-003, M-6, M-17, M-33, M-41, M-35 and M-36) were crushed with an agate mill to a 200-mesh size. A Phillips PW X-ray fluorescence spectrometer (XRF-2400) manufactured in Burladingen, Germany, was used to quantify major element abundances (weight percent). For major element analysis, 50 mg of powder from each sample was dissolved in HF and HNO₃ solution within capped Savillex Teflon breakers. Afterward they were kept in an oven for 48 h at ~190 °C. For trace element analysis, at first the sample powder (0.5 g) was mixed with 5 g of Li₂B₄O₇ to prepare a homogeneous glass disk. Each disk was further analyzed with an AXIOS mineral spectrometer manufactured in CA, USA with an analytical uncertainty of <5% ($\pm 1\sigma$). Loss on ignition (LOI) was obtained by weighing after 1 h of integration at 1000 °C. Thermo XII inductively coupled plasma-mass spectrometer (ICP-MS) manufactured in CA, USA was used to measure trace element and rare earth element (REE) concentrations. For internal calibration, pure elements (Rh and Re) were used, and the uncertainties based on the replicate analyses of internal standards were $\pm 5\%$ for REE and $\pm 5\%$ – 10% for trace elements.

4. Results

4.1. Petrographic Analysis

From the petrographic analysis of representative samples from south and middle part of KGR, it is found that the rock specimens primarily contain quartz (60%–80%) in addition to muscovite (5%–10%) and opaque minerals (<10%). The anhedral grains of quartz, ranging in size from 0.3 to 0.5 mm in size, are commonly equant and sporadically elongated or flattened along the schistosity. The grains are commonly fractured and display well-defined suture contacts. Locally, thin flakes of muscovite define the quartz grain boundaries (Figure 3a–d).

The garnet–staurolite schist samples from the northern part of KGR contain staurolite (30%–50%), garnet (10%–18%), muscovite (5%–10%), quartz and feldspar (10%–15%), and other opaque minerals (5%–8%). Garnet crystals occur as porphyroblasts in schist. In addition, muscovite grains are subhedral to euhedral, ranging from 1.5 to 2.5 mm in diameter. All garnet crystals display partings and cracks, indicating deformation during and after crystal growth (Figure 3e). Mylonite gneiss along the Sagaing fault exhibits deformation structures (wavy foliation) in which quartz, biotite, and chlorite appear (Figure 3f). Similarly, the staurolite exhibits high relief, straw-yellow color, whereas its porphyroblasts display a distinct penetrated twinning, and few crystals are black under Plane Polarized light due to their Fe content. The largest staurolite grain is 5 mm long and 1.5 mm wide.

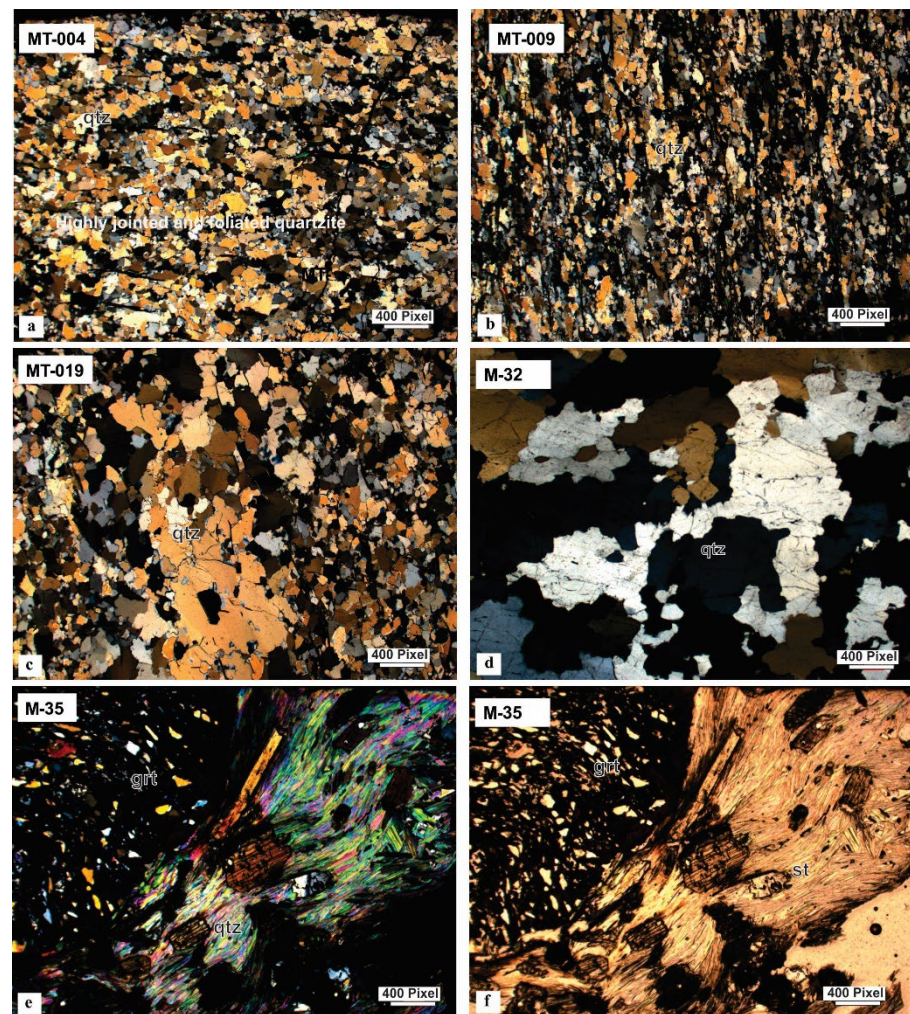


Figure 3. Selected photomicrographs of quartzite samples showing irregular, elongated grains of quartz (a–d), and garnet–staurolite schist samples showing graphite strings and minor biotite and muscovite. In the garnet–staurolite schist sample, there are quartz inclusions in the garnet and kinked micas (e,f). qtz—quartz, grt—garnet, st—staurolite.

4.2. Detrital Zircons U-Pb Results

The zircons of the four samples from the Tigyain area are mostly rounded to sub rounded and have shown oscillatory zoning (Figure 4a). The average Th/U ratio ranges from 0.05 to 2.85, in which dominant numbers of grains have higher value. Thus, the physical appearance and chemical composition indicate the zircons are of igneous origin [65]. Out of 350 analyzed zircon grains, 310 yielded acceptable ages. The U-Pb ages predominantly peak at 634 Ma, 525 Ma, 290 Ma and ~248 Ma, with a subordinate number of grains at 1075 Ma, 916 Ma, 592 Ma, 499 Ma and ~454 Ma. In addition, the ages of several of the grains were clustered at 3394–2717 Ma, and 2490–1734 Ma, and ~1384–719 Ma (Figure 5). The youngest cluster of ages from all four samples: MT-001, MT-004, MT-010 and MT-009 are 518 ± 9 Ma, 471 ± 18 Ma, 273 ± 7 Ma and 248 ± 3 Ma, respectively (Figure 5).

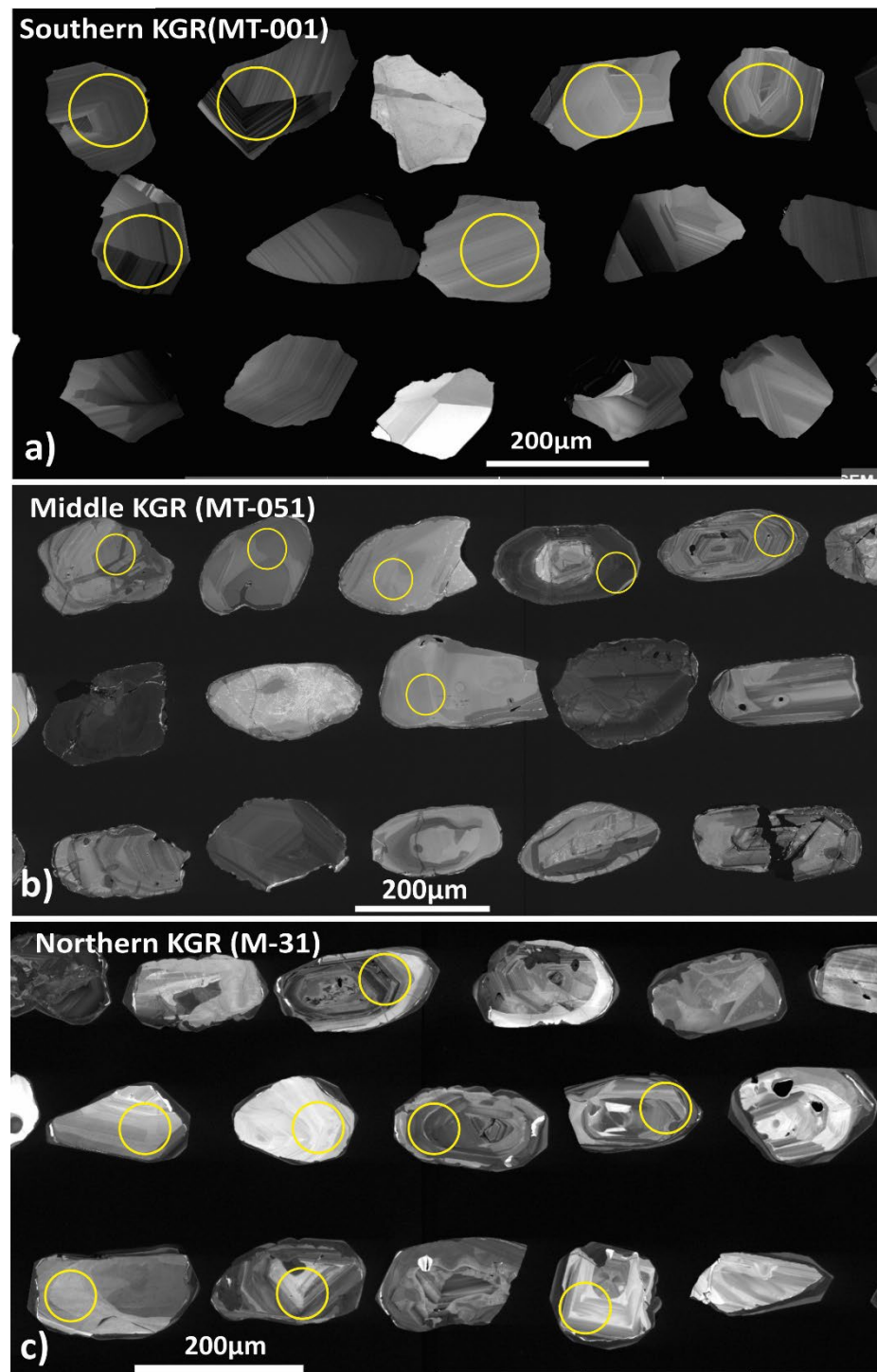


Figure 4. Representative CL image of three regions of the studied area (a) southern, (b) middle and (c) northern KGR. The circle represents the sinter location.

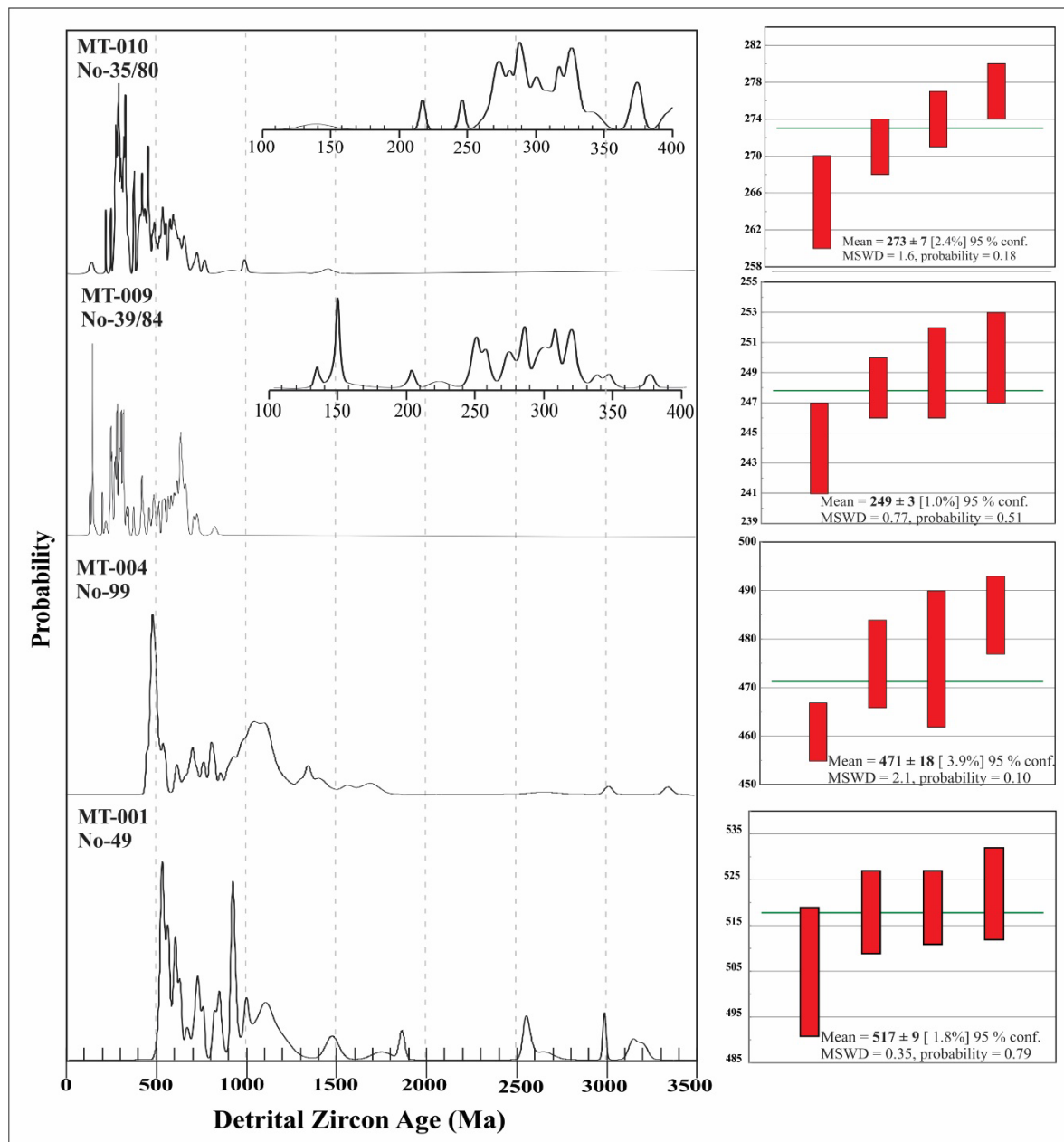


Figure 5. Normalized probability plot of quartzite detrital zircon U-Pb ages from this study, collected from the southernmost section of the Katha-Gangaw range. Samples include MT-001, MT-004, MT-009, and MT-010. No = number of grain analyses in which the denominator indicates the total number, and the numerator indicates the number of grains younger than 400 Ma. The right figure of each sample indicates the maximum depositional age.

From the samples collected from the middle part of KGR, zircon crystals are mostly subangular to rounded (Figure 4b). This morphological characteristic indicates different magmatic zoning: in the inner zone, the pyramidal face is (101), evolving to (211) in the direction of the outer zone in the zircons' zonation in CL images [66,67]. The Th/U ratio range from 0.01 to 2.63 in which the dominating numbers of grains have shown higher value indicating igneous origin [65]. Thus, the physical appearance and chemical composition indicate they are igneous in origin. Among 690 analyses, 509 yielded acceptable ages. The major age populations are in the ranges 1300–750 Ma, 700–450 Ma, and 400–100 Ma, with a small number being subordinate at 3400–2000 Ma (Figure 6). The youngest cluster of ages from the six samples MT-014, MT-019, MT-051, MT-012, MT-047, and MT-045 were

506 ± 8 Ma, 502 ± 7 Ma, 485 ± 7 Ma, 270 ± 3 Ma, 262 ± 3 Ma, and 251 ± 2 Ma, respectively (Figure 6).

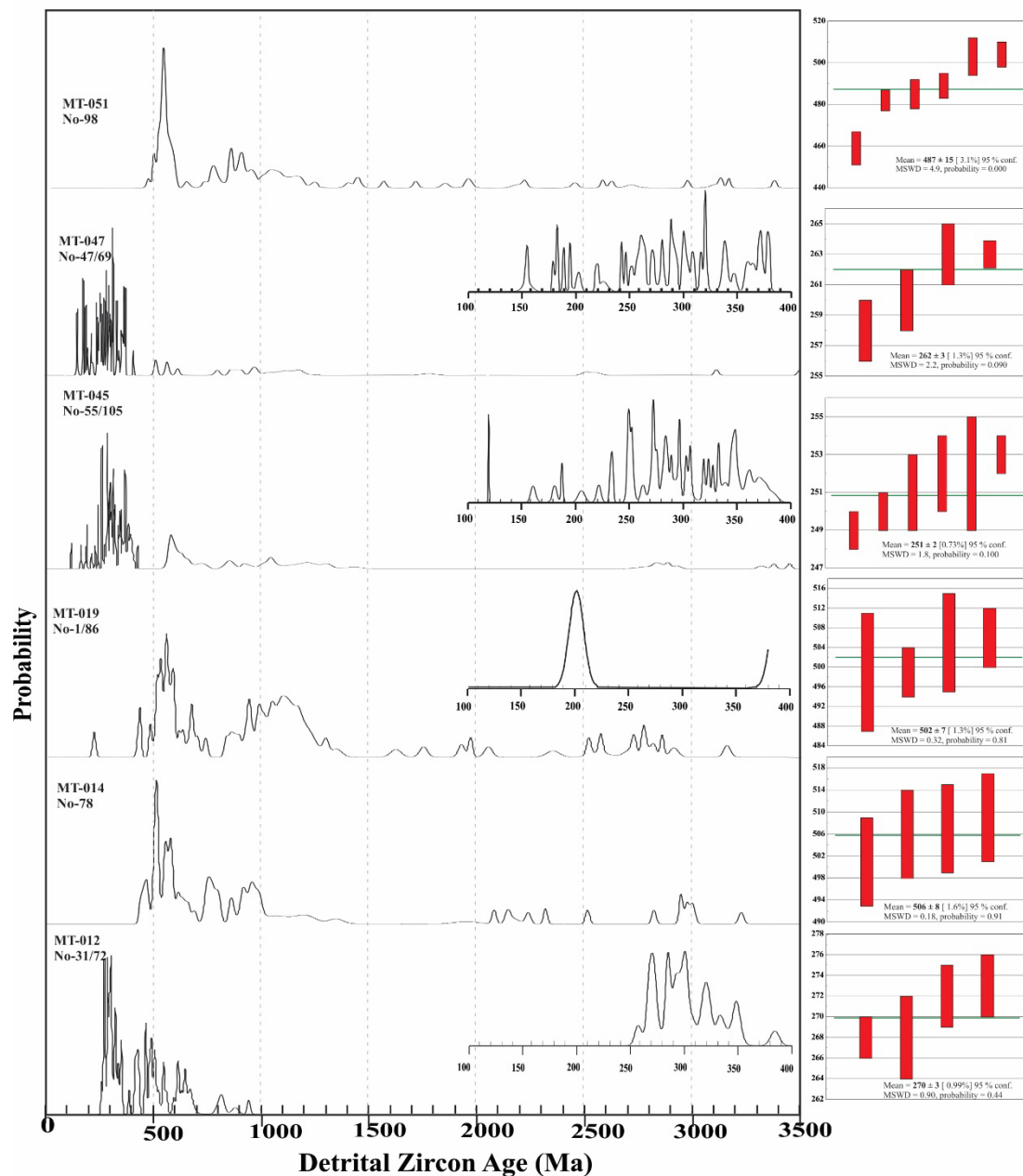


Figure 6. Normalized probability plot of quartzite detrital zircon U-Pb ages from this study, collected from the middle section of the Katha-Gangaw range. Samples include MT-012, MT-014, MT-019, MT-045, MT-047, and MT-051. No = number of grain analyses in which the denominator indicates the total numbers and the numerator indicates the number of grains younger than 400 Ma. The right figure of each sample indicates the maximum depositional age.

The zircon crystals extracted from samples of the northern part of KGR are mostly subangular to rounded (Figure 4c) and yielded Th/U ratios ranging from 0.01 to 2.83, indicating they were predominantly magmatic [65]. The zircons zonation in the CL images yielded different zoning (Figure 4c) such as wavy, faint zoning and some record complex histories involving fracturing and consolidation of broken crystals. Similarly, in this samples also the physical appearance and chemical composition indicate the zircons from northern part of KGR are igneous in origin. Among the 740 analyses, 615 yielded acceptable results.

The major age populations were identified to be in the ranges 750–450 Ma and 400–100 Ma, with subordinate numbers of grains at 3400–2600 Ma, 2500–2200 Ma, and 1200–800 Ma (Figure 7). All U-Pb dating results of the quantitative analyses are displayed in Table S1. The youngest age peak of six samples, MT-025, M-36, M-34, M-35, M-32, M-31, and MT-024A, are 595 ± 8 Ma, 516 ± 5 Ma, 513 ± 5 Ma, 511 ± 7 Ma, 499 ± 5 Ma, 415 ± 5 Ma, and 160 ± 2 Ma, respectively (Figure 7).

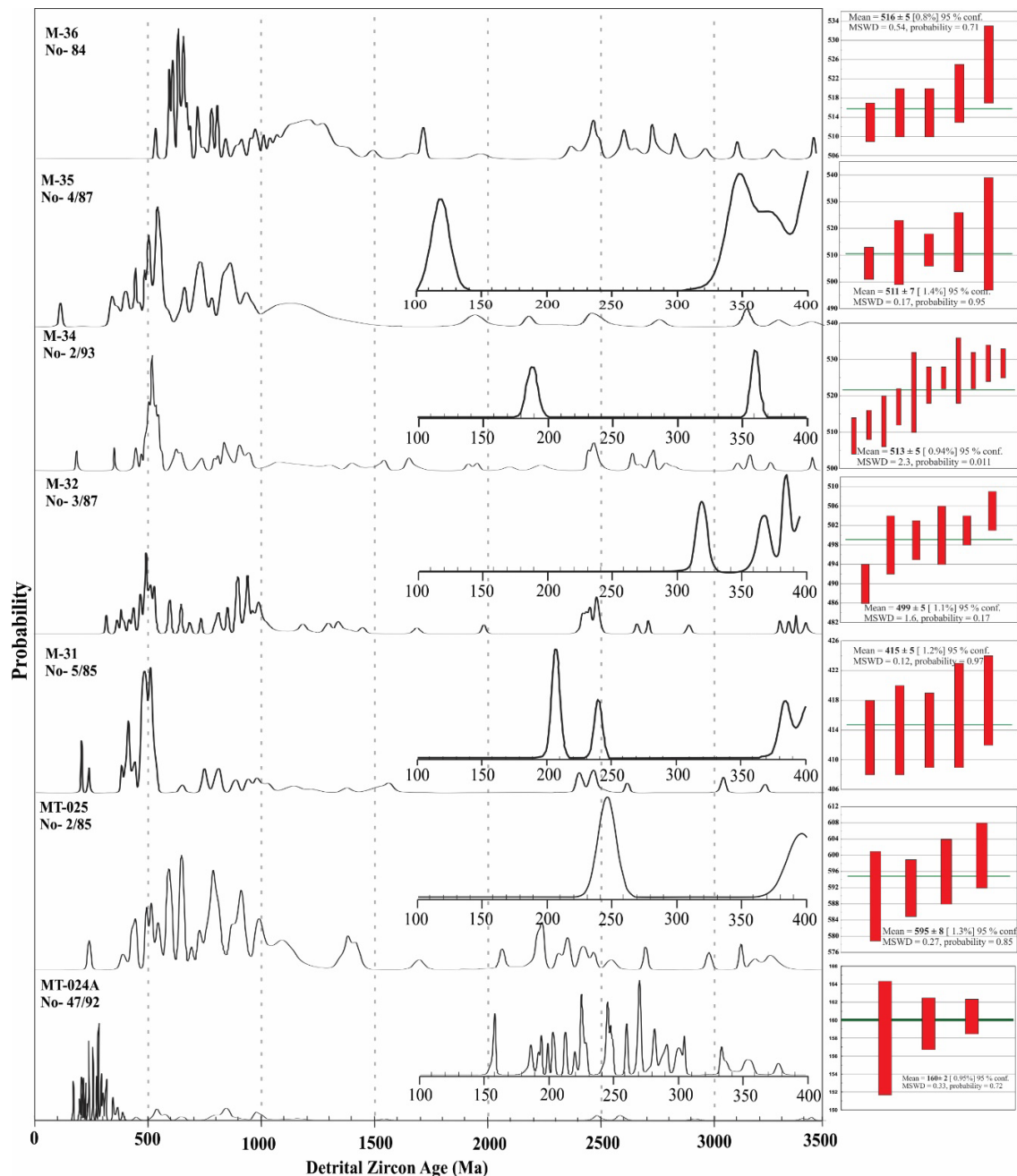


Figure 7. Normalized probability plot of detrital zircon U-Pb ages from this study, collected from the northern section of the Katha-Gangaw range. Samples include MT-024A, MT-025, MT-31, MT-32, and MT-34. Samples M-35 and M-36 are garnet–staurolite schists, whereas all other samples are quartzites. No = number of grain analyses in which the denominator indicates the total number and the numerator indicates the number of grains younger than 400 Ma. The right figure of each sample indicates the maximum depositional age.

4.3. Whole-Rock Geochemistry

The chemical compositions (major, trace, and rare elements) of the studied rock samples from KGR and KR are presented in Table 2. In this study, eight metamorphic rock samples (M-002A, M-003, M-6, M-17, M-33, M-41, M-35, M-36) yielded loss-on-ignition (LOI) values of 0.29–4.18 wt%. The major element values yielded low to high SiO₂ (53.58–84.67 wt.%), and K₂O (0.06–4.28 wt%), MgO (0.30–3.23 wt.%; a single value 6.96 wt%), CaO (0.06 to 3.21 wt.%; one sample value 9.26). Similarly, other elements also yielded low to high values, such as Al₂O₃ (12.21–28.50 wt.%, but one sample showed a lower value of 3.87 wt%), MnO (0.00–0.22 wt%), TiO₂ (0.14–1.98 wt%), Fe₂O₃ (1.48–10.33 wt%), Na₂O (0.11–3.40 wt%, with a single value of 9.40 wt%), P₂O₅ (0.01–0.15 wt%). Detailed results are presented in Table 2. The average (La/Yb)_N ratio of the metamorphosed rocks is 40.75 and this relatively high ratio can be attributed to decrease in HREEs. The (La/Sm)_N ratio of the samples ranges from 3.05–9.21, with an average of 6.86. The (Gd/Yb)_N ratio varies between 1.04–4.69, (one sample of M-33 with a value of 21.56), with an average of 2.84. In addition, the samples display a negative Eu anomaly (Eu/Eu* = 0.46–2.69, average = 0.99; Table 2).

Table 2. Whole-rock major (wt%) and trace element (ppm) compositions of metamorphic rocks in the southernmost part of the Kumon range and Katha-Gangaw range, northern Myanmar.

Sample Unit	M-002A	M-003	M-41	M-6	M-17	M-33	M-35	M-36
SiO ₂	49.37	70.61	74.58	84.67	60.64	58.54	54.87	53.58
TiO ₂	1.98	0.73	0.14	0.22	1.02	1.22	1.18	1.21
Al ₂ O ₃	15.97	13.11	12.21	3.87	18.45	28.50	27.73	27.73
TFe ₂ O ₃	14.96	5.80	1.77	2.86	9.79	3.50	7.95	10.33
MnO	0.22	0.16	0.02	0.17	0.22	0.00	0.01	0.03
MgO	6.96	1.90	0.59	0.71	2.78	0.42	0.30	0.49
CaO	9.27	1.53	0.19	0.17	0.82	0.06	0.11	0.14
Na ₂ O	0.79	1.57	3.40	0.12	0.90	1.33	0.86	1.21
K ₂ O	0.20	2.46	4.29	0.58	4.00	3.22	3.13	2.72
P ₂ O ₅	0.23	0.09	0.03	0.02	0.08	0.03	0.05	0.14
TOTAL	100.26	99.56	98.34	94.43	100.42	100.39	100.39	100.14
LOI	0.30	1.60	1.12	1.04	1.72	3.56	4.18	2.55
FeO	13.46	5.22	1.59	2.57	8.81	3.15	7.16	9.30
Mg	48.21	39.59	39.93	33.18	36.24	19.36	7.11	8.72
K ₂ O + Na ₂ O	0.99	4.03	7.69	0.70	4.90	4.55	3.99	3.93
SiO ₂ /Al ₂ O ₃	3.09	5.39	6.11	21.88	3.29	2.05	1.98	1.93
Sc	26.21	10.24	0.49	4.33	11.68	0.75	0.59	12.20
V	212.88	76.26	11.69	26.23	84.08	130.09	135.39	105.51
Cr	97.43	51.93	3.41	26.99	62.78	83.90	95.77	136.43
Co	40.16	11.61	1.61	5.57	11.94	1.12	8.21	19.47
Ni	41.32	22.66	2.21	10.96	17.67	2.51	38.90	55.94
Cu	24.76	31.10	2.80	10.10	17.07	51.70	22.25	47.73
Zn	114.81	60.56	22.87	14.45	69.80	65.72	47.48	48.79
Rb	11.78	103.45	104.22	22.00	105.45	118.32	119.18	6.21
Sr	62.71	83.98	31.71	7.96	78.49	137.59	112.16	92.01

Table 2. Cont.

Sample Unit	M-002A	M-003	M-41	M-6	M-17	M-33	M-35	M-36
Y	21.67	23.38	17.65	13.77	27.89	2.07	2.79	7.88
Zr	91.29	71.93	205.12	129.48	74.39	224.66	226.92	19.51
Nb	15.89	9.92	15.67	2.61	11.67	30.73	17.87	2.70
Cs	0.26	0.70	0.35	0.14	0.92	4.72	3.82	0.07
Ba	51.21	363.85	463.21	138.46	543.75	789.70	703.29	75.76
La	11.64	31.86	41.70	24.46	41.89	52.25	19.23	4.14
Ce	27.13	57.51	69.41	45.46	82.92	89.74	34.56	9.52
Pr	3.56	6.74	8.79	5.10	9.22	9.39	3.54	1.24
Nd	15.27	24.42	31.17	18.02	33.64	31.90	12.21	5.02
Sm	3.80	4.92	5.94	3.19	6.33	5.67	2.61	1.36
Eu	1.35	1.33	0.92	0.81	1.25	1.13	0.73	0.74
Gd	4.40	5.43	6.04	3.36	6.78	5.42	2.20	1.64
Tb	0.72	0.77	0.78	0.45	0.95	0.47	0.21	0.26
Dy	4.12	4.13	3.81	2.41	5.16	1.18	0.77	1.50
Ho	0.83	0.87	0.73	0.53	1.04	0.13	0.14	0.31
Er	2.36	2.68	2.03	1.60	3.04	0.25	0.38	0.90
Tm	0.33	0.41	0.28	0.24	0.44	0.03	0.05	0.12
Yb	2.18	2.75	1.83	1.60	2.93	0.25	0.35	0.82
Lu	0.32	0.42	0.27	0.23	0.43	0.04	0.05	0.11
Hf	2.43	1.95	6.41	3.25	2.01	5.98	5.92	0.61
Ta	1.33	0.52	0.92	0.15	0.71	2.23	1.26	0.20
Pb	4.57	24.08	21.71	2.46	20.48	34.78	56.01	11.08
Th	0.65	9.20	18.55	10.13	16.39	19.52	18.49	0.16
U	0.39	0.88	2.09	0.61	1.11	2.32	2.54	0.03
(Nb/Ta) _N	11.95	19.13	17.04	17.47	16.42	13.77	14.20	13.68
(Th/Nb) _N	0.58	1.87	0.65	6.27	1.67	0.60	0.01	0.62
(La/Yb) _N	5.33	11.58	22.80	15.25	14.28	207.86	54.17	5.06
(La/Th) _N	17.91	3.46	2.25	2.41	2.56	2.68	1.04	26.25
(Sm/Th) _N	5.84	0.54	0.32	0.32	0.39	0.29	0.14	8.61
(Yb/Th) _N	3.36	0.30	0.10	0.16	0.18	0.01	0.02	5.19
(La/Nb) _N	0.73	3.21	2.66	9.36	3.59	1.70	1.08	1.53
(Nb/Th) _N	24.45	1.08	0.84	0.26	0.71	1.57	0.97	17.14
Eu/Eu*	1.01	0.78	0.47	0.75	0.58	0.61	0.90	1.51

Note: $Eu/Eu^* = (Eu)_N / (Sm + Gd)_N$.

5. Discussion

5.1. Review of U-Pb Data Related to Asian Terranes

Prior to the discussion, a review of the published U-Pb zircon data from Sukhothai terrane, West Papua, Banda arc, Indochina, South Qiangtang terrane, Lhasa terrane, Sibumasu, Tethyan Himalaya, western Myanmar, and Carnarvon basin (Northwest Australia) will strengthen the findings of the present study. Hence, a brief review was done of the published literature on these regions (Figure 8) to discriminate the provenance of Paleozoic–Mesozoic strata in the KGR.

The Sukhothai terrane yielded a broad detrital zircon age distribution ranging from 300 Ma to 180 Ma [3,68]. The detrital zircon U-Pb ages of West Papua clustered between 400 Ma and 200 Ma, with few ages between 2000 Ma and 1500 Ma [69], corresponding with the Upper Triassic strata in the outer Banda arc. The majority of Neoproterozoic (~2.5 Ga), Mesoproterozoic (1.7–1.4 Ga), Grenvillian (~0.95 Ga), and Pan-African (0.65–0.5 Ga) age groups are dominant with a minor Paleo- to Mesoarchean age group in the river sediments of the Truong Son Belt in the Indochina block [70,71]. In the southern Qiangtang terrane, the detrital zircon ages of the Cambrian–Permian strata are similar to those of the Sibumasu terrane. In addition, these strata are characterized by the major age peaks centered at 955 Ma and 558 Ma and smaller peaks at 2470 Ma and 1867 Ma. However, ~2400 Ma–850 Ma, ~500 Ma, ~250 Ma detrital zircons are widely distributed in the Triassic strata of the southern Qiangtang terrane [72–74].

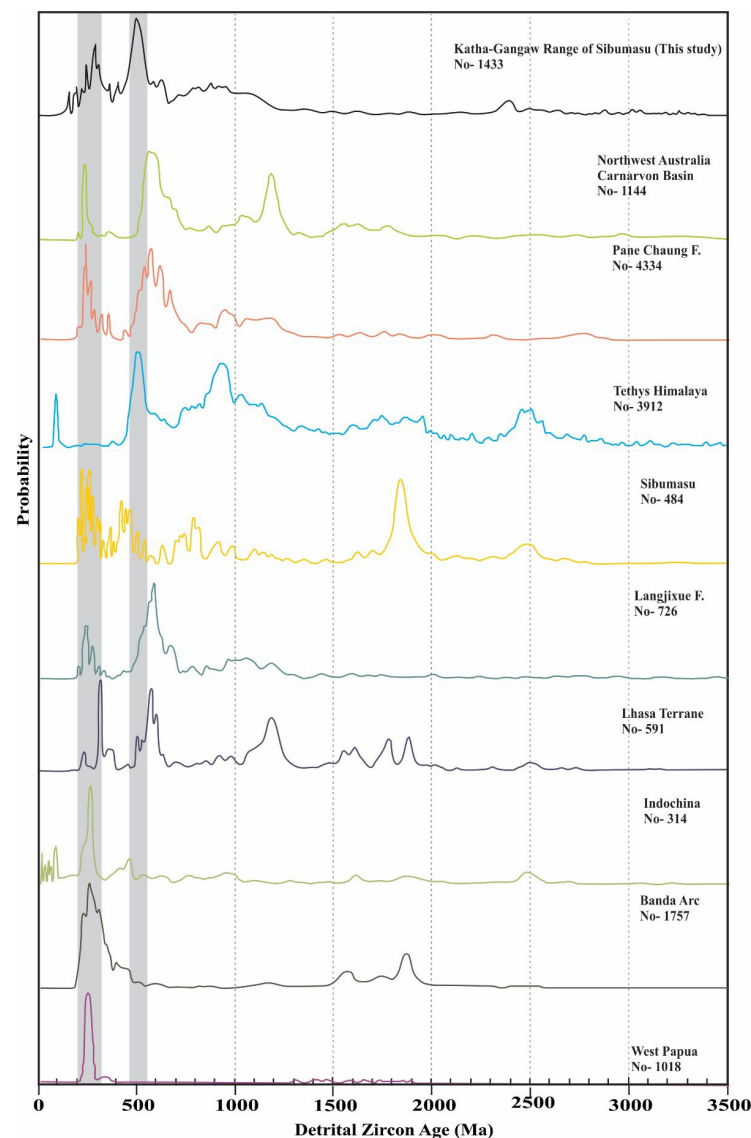


Figure 8. U-Pb age spectra for metamorphic rocks of the Katha-Gangaw range and rocks from the Tethys Himalaya [73,75], Lhasa terrane [76,77], Carnarvon basin of northwestern Australia [78], the Banda arc and West Papua [79], the Langjiexue Formation of southeastern Tibet [80], the Pane Chaung Formation of Myanmar [2,57], Indochina block [70], and Sibumasu block [23]. The grey bar highlights the peak ages corresponding to the adjoining regions.

The Lhasa terrane has a protracted magmatic history that comprises mostly Cretaceous to Paleogene and some Devonian to Jurassic magmatic rocks [81–84]. The pre-Cenozoic sedimentary strata of the Lhasa terrane are dominated by detrital zircon age populations of 1300–800 Ma, 700–500 Ma, 260–180 Ma, and 160–100 Ma, with subordinate numbers of grains between 2000 Ma and 1800 Ma [73,85,86]. The Carboniferous–Permian strata of the Lhasa terrane are characterized by age peaks of about 1188 Ma and 541 Ma, with two subordinate peaks centered about 2694 Ma and 1600 Ma [84]. The Triassic–Jurassic strata in the Lhasa terrane are characterized by age peaks of about 1164 Ma, 564 Ma, and 305 Ma with subordinate peaks within the range of 2500–1500 Ma [87,88].

Similarly, the detrital zircon ages of the Upper Triassic to Lower Jurassic Loi-a Group strata in the Shan Plateau (part of Sibumasu) range from 2000–1700 Ma, 500–400 Ma, and 350–200 Ma [23]. The key age peaks of the Early Permian–Early Jurassic strata in NE India are centered at 2811 Ma, 2482 Ma, 1576 Ma, 952 Ma, and 541 Ma [89]. Detrital zircon ages in Cambrian–Cretaceous strata of the Tethyan Himalaya Sequence are dominated by populations at 2560–2430 Ma, 1200–750 Ma, and 570–480 Ma [73,90]. The Cambrian–Permian Tethyan Himalayan strata are characterized by age peaks at 947 Ma, and 523 Ma, which are broadly distributed between 1200 Ma and 1000 Ma, with two subordinate age peaks at 2535 Ma and 1758 Ma [73,90].

The Upper Triassic Pane Chaung Formation, exposed in the western Myanmar, is dominated by age populations of 1400–700 Ma, 700–500 Ma, and 350–200 Ma, comparable to those of the outer Banda arc [2]. The presence of Carnian–Norian Halobia fossils confirms that the depositional age of this unit ranges between 233 ± 3 Ma and 206 ± 2 Ma [57]. This result is further supported by the presence of ~290–200 Ma detrital zircons in this unit, and those grains were sourced from the West Papua region [57].

The Upper Triassic Mungaroo Formation in the Carnarvon basin, Australia’s north-west shelf, contains four zircon age groups: 1895–1460 Ma (13.9%), 1252–895 Ma (26.6%), 852–455 Ma (39.4%), and 288–199 Ma (5.9%) [78]. The U-Pb age of the Perth basin in southwestern Australia was categorized into three groups [91]: Ordovician strata with peak ages of 1026 Ma and 541 Ma; Permian strata with peak ages of 2617 Ma, 1120 Ma, and 514 Ma; and Triassic with a peak age of 1172 Ma. The zircon from Australia’s Yilgarn Craton peaks between 2.8 and 2.6 Ga and the subordinate numbers of grains are of Permian to Triassic [91,92].

5.2. Tectonics of Myanmar and Adjoining Regions

During the tectonic inversion period, Late Miocene–Pleistocene regional uplift on the eastern side of the Salin Sub-basin in western Myanmar may have controlled volcanic extrusions along reactivated basement-involved normal faults, perpendicular to the NW–SE-trending basin-center thrust/fault [38]. The hyper-oblique convergence of India with western Myanmar was controlled by the collision of Myanmar with Asia during the Miocene [35,38,93]. The convergence between Myanmar and Indian plates took place, and both plates moved towards the north, and onwards of the India–Asia collision, the Indian plate started to rotate anticlockwise [35]. During the Neo-Tethyan subduction, the southern Lhasa terrane experienced three stages of magmatism, in the Jurassic, Cretaceous, and Paleogene [81]. This subduction ended after the collision between the western Myanmar island arc, with the Shan Plateau in the Late Jurassic [4]. The magmatic arcs and accretionary complexes of the Myanmar plate suggest that the long-lived subduction-accretion of the Neo-Tethys Ocean in SE Asia began in the Jurassic. The obtained Triassic to Jurassic ages’ detrital zircons in the studied KGR samples also support this Jurassic tectonic activity. After that, the magmatic arc migrated several times during these accretionary events, including eastward translations (Jurassic to Early Cretaceous, Late Cretaceous to Middle Eocene) and westward translations (Early Cretaceous to Late Early Cretaceous, Middle Eocene to Present) [94].

5.3. Paleogeography of the Gondwana Sibumasu Terrane

During the Late Triassic, the microcontinents were covered by a submarine fan, which was developed along the North Australian shelf between West Papua and Greater India [57]. The Sibumasu terrane was attached with Australia during the Triassic. This result is supported by the fact that the youngest peak age obtained for the stratigraphic succession of KGR (Sibumasu terrane) ranges between 274 ± 3 Ma and 147 ± 2 Ma (present study). The younger age is correlated with the Indo-China block and northwest Australia (Carnarvon basin) (Figure 8). From the detrital zircon ages, it can be postulated that the Paleozoic strata in northern Myanmar have age modes similar to the Gondwanan magmatism, i.e., Grenville (1300–860 Ma), and Pan-African (600–500 Ma). The prominent age peaks at ~1176 and 1070 Ma in the Carboniferous strata indicates that the sources of detritus were Antarctica and Albany–Fraser orogen [1]. Similarly, the Permian–Jurassic and Late Cambrian to Early Ordovician strata in northern Myanmar contain subordinate amounts of Grenville age zircons (1100–900 Ma) [3], which indicates that the Sibumasu terrane was located near the northwestern Australia during Paleozoic. However, the petrographic and detrital zircon *U-Pb* geochronological results of the Ordovician to Lower Jurassic strata within the Sibumasu terrane showed that this terrane was close to the Sukhothai arc during the Early Paleozoic [23]. Hence, we can fairly assume that the Sibumasu terrane was attached to Gondwana during the Paleozoic (Figure 9).

Moreover, the Sibumasu terrane preserves the distinctive Cambrian–Early Permian Gondwanaland fauna of northwest Australian affinities [1,18,19,23,29,95]. A recent paleomagnetic study demonstrated that, the Early Permian Baoshan block (the northern extension of the Sibumasu terrane) was located between the northeast India and northwest Australia [15]. Hence, we can assert that the Sibumasu terrane was situated directly to the east of northwest Australia. The Pane Chaung Formation was deposited on the northwest margin of Australia in the Late Triassic [57]. These findings indicate that, the KGR and KR are a continuation of the IBR. Additionally, the Sibumasu terrane juxtaposed against NW Australia as a part of the Gondwana during the Paleozoic to Early Permian.

The northward movement of the Myanmar plate on the Sagaing fault played a key role in the extension and development of the MMB [4]. Early Eocene sedimentary rocks comprising most of IBR were deposited on the Asian continental margin [35]. It is difficult to constrain the metasediment transport pathways across such a broad paleogeographic region. The strong similarity between the detrital zircon age spectra of quartzites and schists along the length of the Himalaya, implies extraordinary long-distance transport and the extensive mixing of sediment across central Gondwana during the Cambrian–Ordovician [90]. The detrital zircon in Southeast Asia was transported from pre-Gondwana terranes by several fluvial systems across Antarctica, India, and Australia [3]. The extraordinary transport and extensive mixing mechanism is related to the formation of the highland areas during the Pan African and older orogenies. Hence, the study can postulate that the KGR was deposited on the northern Australian margin during the Paleozoic.

5.4. Geochemical Signature

Loss-on-ignition (LOI) values of 0.29–4.18 wt% emphasized low to moderate alteration that was a result of the presence of calcite, quartz, chlorite, and sericite. The metamorphic rocks are enriched in large-ion lithophile elements (LILEs) such as Rb, Cs, Pb, and U, and depleted in high-field-strength elements (HFSEs) such as Nb, Zr, and Ti in the multi-element spider plot diagram. The chondrite-normalized REEs values of the analyzed rocks are slightly enriched in light rare-earth elements (LREEs), while the heavy rare-earth element (HREE) concentrations vary slightly (Figure 10). This result is most similar to upper continental crustal provenance [96]. The negative Eu anomaly might be due to feldspar differentiation and/or crustal contamination of the magma. However, a sample M-036 has shown a positive Eu anomaly which is taken as a premetamorphic signal [97] that could be due to the high temperature (~400 °C) water-rock interaction like seafloor hydrothermal fluids, as well as comparatively lower temperature < 100 °C) interaction [98].

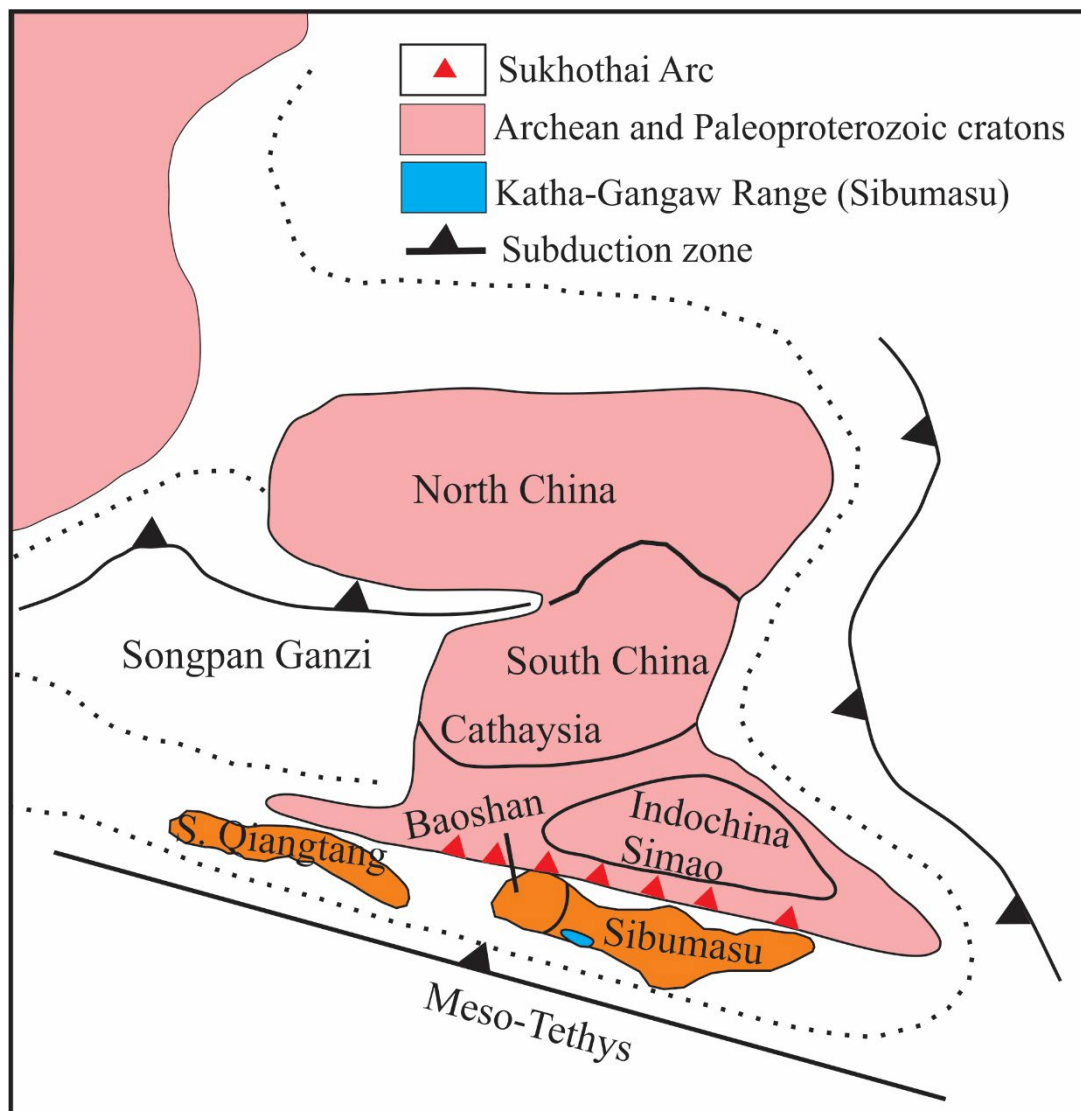


Figure 9. Simplified Late Triassic paleogeographic reconstruction (not to scale) including North China, South China, Indochina, South Qiangtang, and Sibumasu block containing rocks of the Katha-Gangaw Range: modified from [1,23].

The $\text{SiO}_2/\text{Al}_2\text{O}_3 \cdot \text{K}_2\text{O}/\text{Na}_2\text{O}$ ratios (Table 2) suggest that the protoliths of meta-pelitic rocks formed in an arc setting, such as an island arc, as well as active and passive continental margins. According to field observations and petrographic results, these rocks are close to the mineralization boundary; therefore, the effects of mineralized fluid on these rocks could possibly explain the difference. The mineralized fluid may have reduced the amount of SiO_2 in these rocks while increasing H_2O , K_2O , and MgO [99]. Due to the mobility of Na, K, and Ca, it is obvious that there was a considerable weathering process [100]. Caution should be taken when using these components in this kind of interpretation. REE, HFSE, Th, and Sc are more accurate for identifying tectonic settings because they have a low mobility during sedimentary processes and a short residence time in ocean [101].

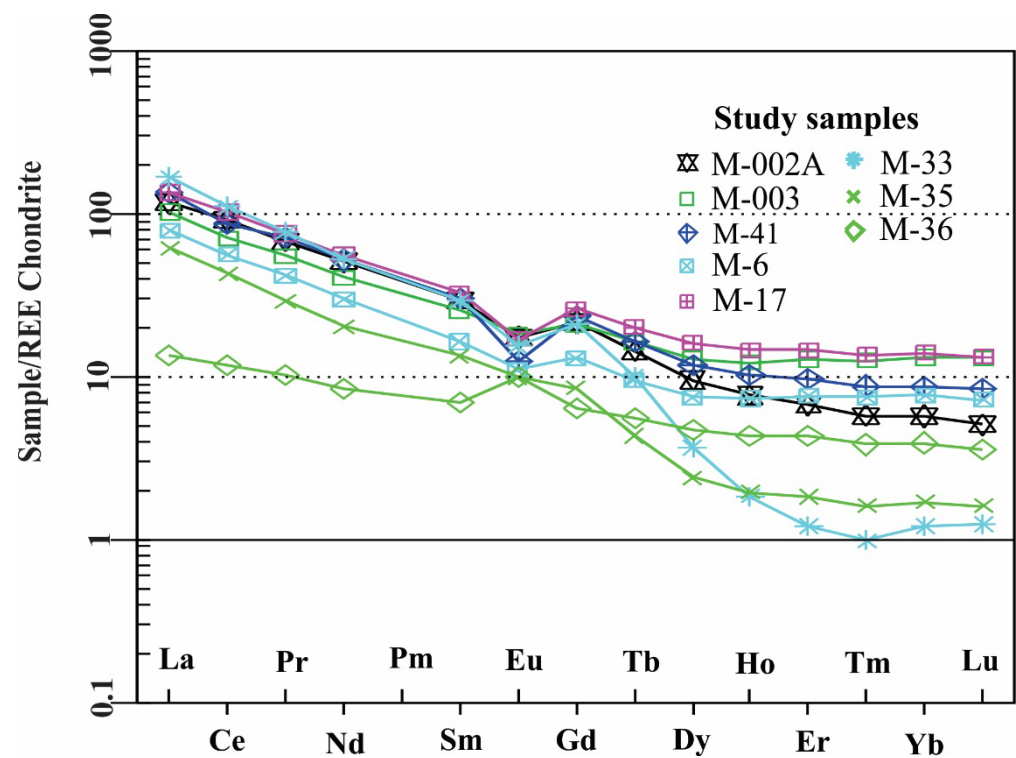


Figure 10. Chondrite-normalized plot of rare-earth element concentrations for rock samples after [99], collected from northern Myanmar. See Table 2 for complete geochemical results.

The Nb/Ta vs. Nb ratio of the study samples shows a depleted mantle source with input of a sediment component in the source area and the Nb/Th vs. La/Nb ratio indicates crustal contamination (Table 2). As is widely known, the continental crust is characterized by a negative Nb anomaly [102]. As a result, crustal contamination depletes Nb as compared to LILE and LREE [103]. A subduction-modified continental lithospheric mantle source possesses high La/Nb (0.73–9.36) and La/Ta (8.75–163.47) ratios, as well as a low La/Ba (0.03–0.23) ratio [104,105]. Sr depletion during metasomatism or metamorphism could be induced by the presence of more calcic plagioclase in the magma source mantle, as well as higher mobility of this element. The concentration of K feldspar and mica in these geological formations controls the Ba anomaly. The relatively low Ce/Y ratios (average 2.79) indicate smaller melt fractions derived from a deeper eruption from the spinel-garnet rich mantle at a depth of 60–90 km [106,107].

The metamorphism in the study area should be tentatively attributed to the Cretaceous to Early Eocene period, with peak conditions occurring in the Early Cretaceous and younger events happening in the Oligocene facies [5,108]. Moreover, the present study findings are consistent with previous works [109–111] that illustrated the source region as modern subduction zones or active continental margins. Please note that the Nb and Zr contents of the metasediments are depleted, indicating a subduction-related, magmatic-arc environment [112].

5.5. Provenance Interpretations

The geochronological ages of the Upper Triassic Pane Chaung Formation (290–200 Ma) in western Myanmar [57] are identical to those of the South Qiangtang terrane 300–200 Ma [80]. In addition, the detrital zircon ages in both Sibumasu and Indochina are identical to the KGR (Figure 8). It has been hypothesized that western Myanmar was the northern continuation of the West Sumatra block (part of Indochina), situated at the southeast margin of Asia [21,29]. Most detrital zircons (west of the Sibumasu terrane) cluster between 350 Ma and 150 Ma, with a peak at 272 Ma (Figure 8). Therefore, the tectonic

evolution of Southeast Asia began prior to the separation from Gondwana. The detrital zircons ranging from 280 Ma to 200 Ma, in Bird's Head terrane of West Papua (Triassic strata) [70], indicate subduction of the Paleo-Pacific plate underneath the Australian plate during the Permian–Triassic. Similar Permian–Triassic detrital zircon groups have been found in the metamorphic and S-type granitoid rocks in northwest Sulawesi [113]. In addition, the Upper Triassic strata in the Banda arc [114,115], Triassic sediments in the Carnarvon basin [78], and Langjiexue Formation and the Tethyan Himalaya [80] were also possible source regions of the KGR (Figure 7). The statistical analysis of younger grains (290–200 Ma) of these three units yielded a comparatively strong relationship with the depositional detrital zircon age of the KGR. Thus, the Permian–Triassic detrital zircons in the KGR were probably derived from the West Papua region. The older grains were derived from the widely exposed Late Neoproterozoic–Cambrian Pan-African and Early Neoproterozoic Grenvillian orogenic belts in western Australia [92,116]. The zircon U-Pb age determined for an ophiolite rock in the Tagaung–Myitkyina ophiolite near the Myitkyina area is 173–171 Ma, similar to the age of the Bangong–Nujiang Suture ophiolite [55]. The Sibumasu terrane with the Late Triassic to Early Jurassic S-type granitoids are resultant of the collision between the Sibumasu terrane and Indochina [117], suggesting a Late Triassic collision age [80].

5.6. *Tectonics of the Sibumasu–Indochina Collision Zone*

The collision of the Sibumasu terrane with Indochina close to the southeastern Paleo-Tethys Ocean basin shaped the Changning–Menglian–Inthanon suture zone [57]. The obtained U-Pb ages of sediments in KGR from the present study along with the U-Pb zircon ages of the Mailonggang [80] constrain the Sibumasu–Indochina collision age to the Late Triassic (Figure 11). Furthermore, the hypothesis is supported by the appearance of Late Triassic S-type granitoids intruding the Paleo–Tethys suture zone and Sibumasu terrane [2,23,57,117]. The KGR (eastern part), uplifted the MMB and Shan Plateau as a result of the eastward underthrusting of the Indian plate beneath western Myanmar (Figure 11). The Permian to Early Triassic volcanic and plutonic rocks of the eastern peninsular of Malaysia and the volcanic rocks of similar ages in central northern Thailand are evidence of the eastward subducting oceanic lithosphere. This arc was collided with the continental foreland (on the subducting plate) to the west, during the Late Triassic Indonesian orogeny [118]. Please note that the presence of the Early Permian brachiopods and foraminifera indicates cool- or cold-water conditions in the Sibumasu terrane, which further highlights that this terrane was far from the equator; however, the Triassic and Jurassic fauna represent the eastern Tethyan provenance [118].

The eastern belt of the IBR consists of schists and Ladinian to Carnian turbidites, which was regionally thrust by serpentized harzburgites and locally by pillow lavas and hornblende gabbro. The Jurassic–Early Cretaceous collision in the eastern IBR is indicated by the presence of the Jurassic ultrabasic rocks, which were dated as 158 ± 20 Ma [119]. The earliest magmatic age (215 Ma) indicates collisional orogeny (crustal thickening) during or prior to the Late Triassic [80]. The oblique plate convergence and subduction are suggested by folding and thrusting within the IBR and westerly directed thrusts with a dextral movement component in the western part of the central basin. The thrusting might have been accompanied by uplift of the IBR, corresponding the Eocene–Oligocene unconformity in the Cretaceous to Paleocene Inner Myanmar basin. The northward movement of western Myanmar relative to the Shillong Plateau is indicated by the Late Cenozoic northwest-directed overthrust in the Naga Hills [51,120].

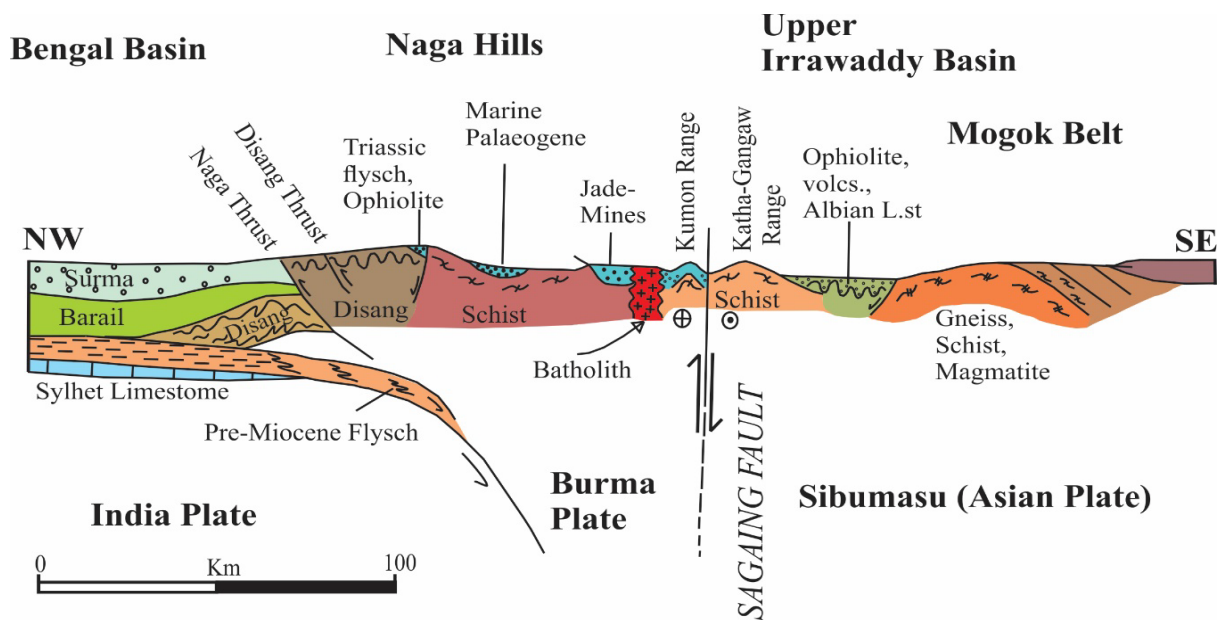


Figure 11. Northwest–southeast-oriented schematic cross section showing the northern Myanmar region during Mesozoic–Cenozoic time. The present-day suture boundary along the Sagaing fault zone along the western margin of the Katha-Gangaw range between western Myanmar and Sibumasu modified after Mitchell [36].

6. Conclusions

The U-Pb detrital zircon ages and geochemical data obtained for the KGR (Sibumasu block/terrane) in northern Myanmar reveal that the rocks exposed in this range were separated from Australia during the Permian to Jurassic. The major conclusions can be summarized as follows:

1. U-Pb detrital zircon ages indicated that the strata of the KGR were deposited on the northwest margin of Australia during the Permian–Triassic, similar to those of the Pane-Chaung Formation and Banda arc. In addition, the KGR and equivalent strata in Greater India, Northwest Australia, and West Papua, comprise a Late Triassic submarine fan that was formed along Australia’s northern border, with a sediment-routing system extending from West Papua to Greater India. Moreover, within Late-Triassic turbidities, significant numbers of Permian–Triassic zircons were identified. The advent of materials from the Permian–Triassic Sukhothai Arc along the western boundary of the Indochina/Simao terrane is required for the drastic change in zircon age spectra. The change in provenance signature from the Gondwana continent to the Sukhothai Arc is assumed to reflect a Late Triassic collision between the Sibumasu and Indochina/Simao terranes.
2. The majority of U-Pb detrital zircon ages from the KGR ranges 1200–822 Ma, 654–388 Ma, and 297–161 Ma is identical to the Tethyan Himalayan sequence. In addition, detrital zircon ages from the Qiangtang terrane further suggests that both units were attached to the Indian and Australian continents during the Ordovician–Silurian. Archean grains were derived from the Albany–Fraser Orogen in NW Australia and the Maud Provinces in Antarctica.
3. In this study, the youngest cluster of ages from KGR range between 274 ± 3 Ma and 147 ± 2 Ma, indicating that the Sibumasu terrane was attached to Australia during the Triassic.
4. Based on geochemical results and a compilation of published constraints, the tectonic evolution of the KGR metasediments are the byproduct of melt and intercalation of crustal materials most probably formed in a forearc setting (subduction-zone) associated with the India–Asia collision. In addition, the current study areas of the

KGR and KR are of arc setting (fore-arc or back-arc basins, adjacent to a volcanic arc developed on the continental crust). Later, during the Pan African orogeny, calc-alkaline magmatism originated from a depleted mantle with crustal contamination, intruded, and crosscut the sedimentary rocks.

Supplementary Materials: The following supporting information can be downloaded at: <https://www.mdpi.com/article/10.3390/min12121632/s1>, Table S1: U-Pb (zircon) geochronological analyses of Katha-Gangaw Range samples.

Author Contributions: Conceptualization, M.M.A. (Myo Myint Aung), F.C. and A.N.T.; Data curation, M.M.A. (Myo Myint Aung), M.M.A. (Me Me Aung), K.S. and K.K.K.; Formal analysis, M.M.A. (Myo Myint Aung) and K.S.; Funding acquisition, L.D.; Investigation, M.M.A. (Myo Myint Aung) and F.C.; Methodology, U.B.; Project administration, L.D. and F.C.; Resources, K.S.; Software, K.K.K.; Supervision, L.D.; Writing—original draft, M.M.A. (Myo Myint Aung), L.D., U.B., F.C., B.N., M.M.A. (Me Me Aung) and A.N.T.; Writing—review & editing, M.M.A. (Myo Myint Aung), L.D. and U.B. All authors have read and agreed to the published version of the manuscript.

Funding: This work was supported by the Chinese Academy of Sciences, Strategic Priority Research Program (Grant No. XDA20070301), the Second Tibetan Plateau Scientific Expedition and Research Program (Grant No. 2019QZKK0708), and the National Natural Science Foundation of China BSCTPES project (Grant No. 41988101). The first author is thankful to the Chinese Government Scholarship's fellowship. The corresponding author is supported by the Chinese Academy of Sciences PIFI-Young Staff Fellowship.

Data Availability Statement: Available online.

Acknowledgments: The authors are grateful to Yahui Yue for her assistance with LA-ICP-MS, U-Pb zircon dating, and Than Zaw for his help during the fieldwork.

Conflicts of Interest: The authors declare no conflict of interest.

References

1. Metcalfe, I. Gondwana dispersion and Asian accretion: Tectonic and palaeogeographic evolution of eastern Tethys. *J. Asian Earth Sci.* **2013**, *66*, 1–33. [[CrossRef](#)]
2. Sevastjanova, I.; Hall, R.; Rittner, M.; Paw, S.M.T.L.; Naing, T.T.; Alderton, D.H.; Comfort, G.; Paw, S.M.T.L.; Naing, T.T.; Alderton, D.H.; Comfort, G. Myanmar and Asia united, Australia left behind long ago. *Gondwana Res.* **2015**, *32*, 24–40. [[CrossRef](#)]
3. Burrett, C.; Khin, Z.; Meffre, S.; Lai, C.K.; Khositanont, S.; Chaodumrong, P.; Udchachon, M.; Ekins, S.; Halpin, J. The configuration of Greater Gondwana—Evidence from LA ICPMS, U-Pb geochronology of detrital zircons from the Palaeozoic and Mesozoic of Southeast Asia and China. *Gondwana Res.* **2014**, *26*, 31–51. [[CrossRef](#)]
4. Mitchell, A.H.G.; Htay, M.T.; Htun, K.M.; Win, M.N.; Oo, T.; Hlaing, T. Rock relationships in the Mogok metamorphic belt, Tatkon to Mandalay, central Myanmar. *J. Asian Earth Sci.* **2007**, *29*, 891–910. [[CrossRef](#)]
5. Win, T.P.; Nu, T.T.; Thin, A.K. Mineral Assemblages and Metamorphic Condition of The Katha Metamorphics Exposed In Katha-Indaw Area, Sagaing Region, Myanmar. In Proceedings of the First Myanmar National Conference on Earth Sciences (MNCES, 2017), University of Monywa, Monywa, Myanmar, 27–28 November 2017.
6. Yin, A.; Harrison, T.M. Geologic evolution of the Himalayan-Tibetan orogen. *Annu. Rev. Earth Planet. Sci.* **2000**, *28*, 211–280. [[CrossRef](#)]
7. Bannert, D.; Sang Lyen, A.; Htay, T. The geology of the Indo Burma Ranges in Myanmar. *Schweiz. Sci.* **2011**, *3A*, 101.
8. Bertrand, G.; Rangin, C. Tectonics of the western margin of the Shan plateau (central Myanmar): Implication for the India-Indochin oblique convergence since the Oligocene. *J. Asian Earth Sci.* **2003**, *21*, 1139–1157. [[CrossRef](#)]
9. Curray, J.R. Tectonics and history of the Andaman Sea region. *J. Asian Earth Sci.* **2005**, *25*, 187–232. [[CrossRef](#)]
10. Vigny, C.; Socquet, A.; Rangin, C.; Chamot-Rooke, N.; Pubellier, M.; Bouin, M.-N.; Bertrand, G.; Becker, M. Present-day crustal deformation around Sagaing fault, Myanmar. *J. Geophys. Res. Solid Earth* **2003**, *108*, 1–10. [[CrossRef](#)]
11. Bunopas, S.; Vella, P. Tectonic and geologic evolution of Thailand. In Proceedings of the Workshop on Stratigraphic Correlation of Thailand and Malaysia, Haad Yai, Thailand, 8–10 September 1983; pp. 307–322.
12. Dickinson, W.R.C.J.; Ingersoll, R.; Tankard, A. In Tectonics of sedimentary basins. *Sediment. Geol.* **1995**, *106*, 301–302.
13. Noda, A. Forearc basins: Types, geometries, and relationships to subduction zone dynamics. *Bulletin* **2016**, *128*, 879–895. [[CrossRef](#)]
14. Orme, D.A.; Laskowski, A.K. Basin Analysis of the Albian–Santonian Xigaze Forearc, Lazi Region, South-Central Tibet. *J. Sediment. Res.* **2016**, *86*, 894–913. [[CrossRef](#)]

15. Ali, J.; Cheung, H.; Aitchison, J.; Sun, Y. Palaeomagnetic re-investigation of Early Permian rift basalts from the Baoshan Block, SW China: Constraints on the site-of-origin of the Gondwana-derived eastern Cimmerian terranes. *Geophys. J. Int.* **2013**, *193*, 650–663. [[CrossRef](#)]
16. Hall, R. Cenozoic geological and plate tectonic evolution of SE Asia and the SW Pacific: Computer-based reconstructions, model and animations. *J. Asian Earth Sci.* **2002**, *20*, 353–431. [[CrossRef](#)]
17. Hall, R.; Sevastjanova, I. Australian crust in Indonesia. *Aust. J. Earth Sci.* **2012**, *59*, 827–844. [[CrossRef](#)]
18. Metcalfe, I. Pre-Cretaceous evolution of SE Asian terranes. *Geol. Soc. Lond. Spec. Publ.* **1996**, *106*, 97–122. [[CrossRef](#)]
19. Metcalfe, I. Gondwanaland dispersion, Asian accretion and evolution of eastern Tethys. *Aust. J. Earth Sci.* **1996**, *43*, 605–623. [[CrossRef](#)]
20. Metcalfe, I. Palaeozoic and Mesozoic tectonic evolution and palaeogeography of East Asian crustal fragments: The Korean Peninsula in context. *Gondwana Res.* **2006**, *9*, 24–46. [[CrossRef](#)]
21. Barber, A.J.; Crow, M.J. Structure of Sumatra and its implications for the tectonic assembly of Southeast Asia and the destruction of Paleotethys. *Isl. Arc* **2009**, *18*, 3–20. [[CrossRef](#)]
22. Metcalfe, I. The Bentong–Raub Suture Zone. *J. Asian Earth Sci.* **2000**, *18*, 691–712. [[CrossRef](#)]
23. Cai, F.; Ding, L.; Yao, W.; Laskowski, A.K.; Xu, Q.; Zhang, J.E.; Sein, K. Provenance and tectonic evolution of Lower Paleozoic–Upper Mesozoic strata from Sibumasu terrane, Myanmar. *Gondwana Res.* **2017**, *41*, 325–336. [[CrossRef](#)]
24. Cai, F.; Ding, L.; Leary, R.J.; Wang, H.; Xu, Q.; Zhang, L.; Yue, Y. Tectonostratigraphy and provenance of an accretionary complex within the Yarlung–Zangpo suture zone, southern Tibet: Insights into subduction—Accretion processes in the Neo-Tethys. *Tectonophysics* **2012**, *574*, 181–192. [[CrossRef](#)]
25. Kyaw Linn, O.; Khin, Z.; Meffre, S.; Aung, D.W.; Lai, C.-K. Provenance of the Eocene sandstones in the southern Chindwin Basin, Myanmar: Implications for the unroofing history of the Cretaceous–Eocene magmatic arc. *J. Asian Earth Sci.* **2015**, *107*, 172–194. [[CrossRef](#)]
26. Lin, N.H.; Guo, Y.; Wai, S.N.; Tamehe, L.S.; Wu, Z.; Naing, N.M.; Zhang, J. Sedimentology and geochemistry of Middle Eocene–Lower Oligocene sandstones from the western Salin Sub-Basin, the Central Myanmar Basin: Implications for provenance, source area weathering, paleo-oxidation and paleo-tectonic setting. *J. Asian Earth Sci.* **2019**, *173*, 314–335. [[CrossRef](#)]
27. Thein, M.; Maung, M. The Eastern (Back-arc) Basin of Central Myanmar: Basement rocks, lithostratigraphic units, palaeocurrents, provenance and developmental history. *Geol. Soc. Lond. Mem.* **2017**, *48*, 169–183. [[CrossRef](#)]
28. Westerweel, J.; Roperch, P.; Licht, A.; Dupont-Nivet, G.; Win, Z.; Poblete, F.; Ruffet, G.; Swe, H.H.; Thi, M.K.; Aung, D.W. Burma Terrane part of the Trans-Tethyan arc during collision with India according to palaeomagnetic data. *Nat. Geosci.* **2019**, *12*, 863–868. [[CrossRef](#)]
29. Metcalfe, I. Palaeozoic–Mesozoic history of SE Asia. *Geol. Soc. Lond. Spec. Publ.* **2011**, *355*, 7–35. [[CrossRef](#)]
30. Bannert, D.; Helmcke, D. The evolution of the Asian Plate in Burma. *Geol. Rundsch.* **1981**, *70*, 446–458. [[CrossRef](#)]
31. Li, R.; Mei, L.; Zhu, G.; Zhao, R.; Xu, X.; Zhao, H.; Zhang, P.; Yin, Y.; Ma, Y. Late mesozoic to cenozoic tectonic events in volcanic arc, West Burma Block: Evidences from U-Pb zircon dating and apatite fission track data of granitoids. *J. Earth Sci.* **2013**, *24*, 553–568. [[CrossRef](#)]
32. Cai, F.; Ding, L.; Yue, Y. Provenance analysis of upper Cretaceous strata in the Tethys Himalaya, southern Tibet: Implications for timing of India–Asia collision. *Earth Planet. Sci. Lett.* **2011**, *305*, 195–206. [[CrossRef](#)]
33. Garzanti, E.; Padoan, M.; Andò, S.; Resentini, A.; Vezzoli, G.; Lustrino, M. Weathering and relative durability of detrital minerals in equatorial climate: Sand petrology and geochemistry in the East African Rift. *J. Geol.* **2013**, *121*, 547–580. [[CrossRef](#)]
34. Myrow, P.M.; Hughes, N.C.; Goodge, J.W.; Fanning, C.M.; Williams, I.S.; Peng, S.; Bhargava, O.N.; Parcha, S.K.; Pogue, K.R. Extraordinary transport and mixing of sediment across Himalayan central Gondwana during the Cambrian–Ordovician. *Bulletin* **2010**, *122*, 1660–1670. [[CrossRef](#)]
35. Mitchell, A.H.G. Cretaceous–Cenozoic tectonic events in the western Myanmar (Burma)–Assam region. *J. Geol. Soc.* **1993**, *150*, 1089–1102. [[CrossRef](#)]
36. Metcalfe, I.; Kyi Pyar, A. Late Tournaisian conodonts from the Taungnyo Group near Loi Kaw, Myanmar (Burma): Implications for Shan Plateau stratigraphy and evolution of the Gondwana-derived Sibumasu Terrane. *Gondwana Res.* **2014**, *26*, 1159–1172. [[CrossRef](#)]
37. Mitchell, A.; Chung, S.-L.; Oo, T.; Lin, T.-H.; Hung, C.-H. Zircon U-Pb ages in Myanmar: Magmatic–metamorphic events and the closure of a neo-Tethys ocean? *J. Asian Earth Sci.* **2012**, *56*, 1–23. [[CrossRef](#)]
38. Pivnik, D.A.; Nahm, J.; Tucker, R.S.; Smith, G.O.; Nyein, K.; Nyunt, M.; Maung, P.H. Polyphase deformation in a fore-arc/back-arc basin, Salin subbasin, Myanmar (Burma). *AAPG Bull.* **1998**, *82*, 1837–1856.
39. Thaire Phyu, W. Petrology of the Katha Metamorphics between Indaw and Katha, Sagaing Region. Ph.D. Thesis, University of Mandalay, Mandalay, Myanmar, 2011.
40. Ridd, M.F. South-East Asia as a Part of Gondwanaland. *Nature* **1971**, *234*, 531–533. [[CrossRef](#)]
41. Metcalfe, I. Origin and assembly of south-east Asian continental terranes. *Geol. Soc. Lond. Spec. Publ.* **1988**, *37*, 101–118. [[CrossRef](#)]
42. Mitchell, A. Tectonic settings for emplacement of Southeast Asian tin granites. *Geol. Soc. Malays. Bull.* **1977**, *9*, 123–140. [[CrossRef](#)]
43. Boucot, A.J. Some thoughts about the Shan–Thai terrane. *War. Geol.* **2003**, *29*, 1–11.
44. Bender, F. *Geology of Burma*; Gebrüder Bornträger Verlagsbuchhandlung: Berlin, Germany; Stuttgart, Germany, 1983.

45. Mitchell, A.H.G. Late Permian-Mesozoic events and the Mergui group Nappe in Myanmar and Thailand. *J. Southeast Asian Earth Sci.* **1992**, *7*, 165–178. [[CrossRef](#)]
46. Searle, M.; Noble, S.; Cottle, J.; Waters, D.; Mitchell, A.; Hlaing, T.; Horstwood, M. Tectonic evolution of the Mogok metamorphic belt, Burma (Myanmar) constrained by U-Th-Pb dating of metamorphic and magmatic rocks. *Tectonics* **2007**, *26*, 1–24. [[CrossRef](#)]
47. Barber, A.; Crow, M. An evaluation of plate tectonic models for the development of Sumatra. *Gondwana Res.* **2003**, *6*, 1–28. [[CrossRef](#)]
48. Khin, K. Marine transgression and regression in Miocene sequences of northern Pegu (Bago) Yoma, central Myanmar. *J. Asian Earth Sci.* **1999**, *17*, 369–393. [[CrossRef](#)]
49. Mitchell, A. *Geological Belts, Plate Boundaries, and Mineral Deposits in Myanmar*; Elsevier: Amsterdam, The Netherlands, 2018.
50. Wang, J.-G.; Wu, F.-Y.; Tan, X.-C.; Liu, C.-Z. Magmatic evolution of the Western Myanmar Arc documented by U-Pb and Hf isotopes in detrital zircon. *Tectonophysics* **2014**, *612*, 97–105. [[CrossRef](#)]
51. Curray, J.; Moore, D.; Lawver, L.; Emmel, F.; Raitt, R.; Henry, M.; Kieckhefer, R. Tectonics of the Andaman Sea and Burma: Convergent margins. In *M 29: Geological and Geophysical Investigations of Continental Margins*; Special Volumes; AAPG: Tulsa, OK, USA, 1979; pp. 189–198.
52. Hutchison, C.S. *Geological Evolution of South-East Asia*; Oxford University Press: Oxford, UK, 1989; Volume 13, p. 368.
53. Trevena, A.; Varga, R.; Collins, I.; Nu, U. *Tertiary Tectonics and Sedimentation in the Salin (Fore-arc) Basin, Myanmar*; AAPG Bulletin; American Association of Petroleum Geologists: Tulsa, OK, USA, 1991; Volume 75.
54. Swe, W. A major strike-slip fault in Burma. *Contrib. Burmese Geol.* **1981**, *1*, 63–72.
55. Liu, C.-Z.; Chung, S.-L.; Wu, F.-Y.; Zhang, C.; Xu, Y.; Wang, J.-G.; Chen, Y.; Guo, S. Tethyan suturing in Southeast Asia: Zircon U-Pb and Hf-O isotopic constraints from Myanmar ophiolites. *Geology* **2016**, *44*, 311–314. [[CrossRef](#)]
56. Mitchell, A. The Chin Hills segment of the Indo-Burman Ranges: Not a simple accretionary wedge. In Proceedings of the Seminar on Indo-Myanmar Ranges in the Tectonic Framework of the Himalaya and Southeast Asia, Conchipur, India, 27–29 November 2008; Manipur University: Conchipur, India, 2008; pp. 3–24.
57. Yao, W.; Ding, L.; Cai, F.; Wang, H.; Xu, Q.; Zaw, T. Origin and tectonic evolution of upper Triassic Turbidites in the Indo-Burman ranges, West Myanmar. *Tectonophysics* **2017**, *721*, 90–105. [[CrossRef](#)]
58. Maung, M.; Thu, A.N.; Suzuki, H.; Swe, W.; Tun, S.T.; Thant, M.; Zaw, K. Latest Jurassic radiolarian fauna from the Chinghkrana area, Myitkyina township, Kachin state, northern Myanmar. In *Regional Congress on Mineral and Energy Resources of Southeast Asia*; GEOSEA: Yangon, Myanmar, 2014; pp. 38–39.
59. Lin, D.; Goswami, T.K.; Fulong, C.; Baral, U.; Sarmah, R.K.; Bezbaruah, D. Detrital zircon U-Pb ages of Tertiary sequences (Palaeocene-Miocene): Inner Fold Belt and Belt of Schuppen, Indo-Myanmar Ranges, India. *Geol. J.* **2022**, 1–16. [[CrossRef](#)]
60. Wu, F.-Y.; Clift, P.D.; Yang, J.-H. Zircon Hf isotopic constraints on the sources of the Indus Molasse, Ladakh Himalaya, India. *Tectonics* **2007**, *26*, 1–15. [[CrossRef](#)]
61. Sláma, J.; Košler, J.; Condon, D.J.; Crowley, J.L.; Gerdes, A.; Hanchar, J.M.; Horstwood, M.S.; Morris, G.A.; Nasdala, L.; Norberg, N. Plešovice zircon—A new natural reference material for U-Pb and Hf isotopic microanalysis. *Chem. Geol.* **2008**, *249*, 1–35. [[CrossRef](#)]
62. Andersen, T. Correction of common lead in U-Pb analyses that do not report 204Pb. *Chem. Geol.* **2002**, *192*, 59–79. [[CrossRef](#)]
63. Dickinson, W.R.; Gehrels, G.E. Use of U-Pb ages of detrital zircons to infer maximum depositional ages of strata: A test against a Colorado Plateau Mesozoic database. *Earth Planet. Sci. Lett.* **2009**, *288*, 115–125. [[CrossRef](#)]
64. Vermeesch, P. Maximum depositional age estimation revisited. *Geosci. Front.* **2021**, *12*, 843–850. [[CrossRef](#)]
65. Rubatto, D. Zircon trace element geochemistry: Partitioning with garnet and the link between U-Pb ages and metamorphism. *Chem. Geol.* **2002**, *184*, 123–138. [[CrossRef](#)]
66. Martins, H.C.B.; Simões, P.P.; Abreu, J. Zircon crystal morphology and internal structures as a tool for constraining magma sources: Examples from northern Portugal Variscan biotite-rich granite plutons. *Comptes Rendus Geosci.* **2014**, *346*, 233–243. [[CrossRef](#)]
67. Hoskin, P.W.O.; Schaltegger, U. The Composition of Zircon and Igneous and Metamorphic Petrogenesis. *Rev. Mineral. Geochem.* **2003**, *53*, 27–62. [[CrossRef](#)]
68. Sevastjanova, I.; Clements, B.; Hall, R.; Belousova, E.; Griffin, W.; Pearson, N. Granitic magmatism, basement ages, and provenance indicators in the Malay Peninsula: Insights from detrital zircon U-Pb and Hf-isotope data. *Gondwana Res.* **2011**, *19*, 1024–1039. [[CrossRef](#)]
69. Gunawan, I.; Hall, R.; Sevastjanova, I. Age, character and provenance of the Tipuma Formation, West Papua: New insights from detrital zircon dating. In Proceedings of the Indonesian Petroleum Association, 36th Annual Convention, Jakarta, Indonesia, 23–25 May 2012.
70. Usuki, T.; Lan, C.-Y.; Wang, K.-L.; Chiu, H.-Y. Linking the Indochina block and Gondwana during the Early Paleozoic: Evidence from U-Pb ages and Hf isotopes of detrital zircons. *Tectonophysics* **2013**, *586*, 145–159. [[CrossRef](#)]
71. Wang, J.-G.; Wu, F.-Y.; Garzanti, E.; Hu, X.; Ji, W.-Q.; Liu, Z.-C.; Liu, X.-C. Upper Triassic turbidites of the northern Tethyan Himalaya (Langjiexue Group): The terminal of a sediment-routing system sourced in the Gondwanide Orogen. *Gondwana Res.* **2016**, *34*, 84–98. [[CrossRef](#)]

72. Ding, L.; Yang, D.; Cai, F.L.; Pullen, A.; Kapp, P.; Gehrels, G.E.; Zhang, L.Y.; Zhang, Q.H.; Lai, Q.Z.; Yue, Y.H.; et al. Provenance analysis of the Mesozoic Hoh-Xil-Songpan-Ganzi turbidites in northern Tibet: Implications for the tectonic evolution of the eastern Paleo-Tethys Ocean. *Tectonics* **2013**, *32*, 34–48. [[CrossRef](#)]
73. Gehrels, G.; Kapp, P.; DeCelles, P.; Pullen, A.; Blakey, R.; Weislogel, A.; Ding, L.; Guynn, J.; Martin, A.; McQuarrie, N.; et al. Detrital zircon geochronology of pre-Tertiary strata in the Tibetan-Himalayan orogen. *Tectonics* **2011**, *30*, TC5016. [[CrossRef](#)]
74. Pullen, A.; Kapp, P.; Gehrels, G.E.; Vervoort, J.D.; Ding, L. Triassic continental subduction in central Tibet and Mediterranean-style closure of the Paleo-Tethys Ocean. *Geology* **2008**, *36*, 351–354. [[CrossRef](#)]
75. DeCelles, P.; Gehrels, G.; Quade, J.; LaReau, B.; Spurlin, M. Tectonic implications of U-Pb zircon ages of the Himalayan orogenic belt in Nepal. *Science* **2000**, *288*, 497–499. [[CrossRef](#)]
76. Li, Y.; Wang, C.; Dai, J.; Xu, G.; Hou, Y.; Li, X. Propagation of the deformation and growth of the Tibetan-Himalayan orogen: A review. *Earth-Sci. Rev.* **2015**, *143*, 36–61. [[CrossRef](#)]
77. Li, X.-H.; Li, Z.-X.; Li, W.-X. Detrital zircon U-Pb age and Hf isotope constrains on the generation and reworking of Precambrian continental crust in the Cathaysia Block, South China: A synthesis. *Gondwana Res.* **2014**, *25*, 1202–1215. [[CrossRef](#)]
78. Lewis, C.; Sircombe, K.; Keep, M.; Moss, S. Use of U-Pb geochronology to delineate provenance of North West Shelf sediments, Australia. In *The Sedimentary Basins of Western Australia IV: Proceedings of the Petroleum Exploration Society of Australia Symposium, Perth, Australia, 18–21 August 2013*; Petroleum Exploration Society of Australia: Perth, Australia, 2013; pp. 1–27.
79. Bird, P.R.; Cook, S.E. Permo-Triassic successions of the Kerkennah area, West Timor: Implications for palaeogeography and basin evolution. *J. Southeast Asian Earth Sci.* **1991**, *6*, 359–371. [[CrossRef](#)]
80. Cai, F.; Ding, L.; Laskowski, A.K.; Kapp, P.; Wang, H.; Xu, Q.; Zhang, L. Late Triassic paleogeographic reconstruction along the Neo-Tethyan Ocean margins, southern Tibet. *Earth Planet. Sci. Lett.* **2016**, *435*, 105–114. [[CrossRef](#)]
81. Chu, M.-F.; Chung, S.-L.; Song, B.; Liu, D.; O'Reilly, S.Y.; Pearson, N.J.; Ji, J.; Wen, D.-J. Zircon U-Pb and Hf isotope constraints on the Mesozoic tectonics and crustal evolution of southern Tibet. *Geology* **2006**, *34*, 745–748. [[CrossRef](#)]
82. Ji, W.-Q.; Wu, F.-Y.; Chung, S.-L.; Liu, C.-Z. Identification of early Carboniferous granitoids from southern Tibet and implications for terrane assembly related to the Paleo-Tethyan evolution. *J. Geol.* **2012**, *120*, 531–541. [[CrossRef](#)]
83. Zhang, R.; Xu, W.; Guo, J.; Zong, K.; Cai, H.; Yuan, H. Zircon U-Pb and Hf isotopic composition of deformed granite in the southern margin of the Gangdese belt, Tibet: Evidence for Early Jurassic subduction of Neo-Tethyan oceanic slab. *Acta Petrol. Sin.* **2007**, *23*, 1347–1353.
84. Zhu, D.-C.; Zhao, Z.-D.; Niu, Y.; Mo, X.-X.; Chung, S.-L.; Hou, Z.-Q.; Wang, L.-Q.; Wu, F.-Y. The Lhasa Terrane: Record of a microcontinent and its histories of drift and growth. *Earth Planet. Sci. Lett.* **2011**, *301*, 241–255. [[CrossRef](#)]
85. Leier, A.L.; Kapp, P.; Gehrels, G.E.; DeCelles, P.G. Detrital zircon geochronology of Carboniferous–Cretaceous strata in the Lhasa terrane, Southern Tibet. *Basin Res.* **2007**, *19*, 361–378.
86. Pullen, A.; Kapp, P.; Gehrels, G.E.; DeCelles, P.G.; Brown, E.H.; Fabijanic, J.M.; Ding, L. Gangdese retroarc thrust belt and foreland basin deposits in the Damxung area, southern Tibet. *J. Asian Earth Sci.* **2008**, *33*, 323–336. [[CrossRef](#)]
87. Li, G.; Sandiford, M.; Liu, X.; Xu, Z.; Lijie, W.; Li, H. Provenance of Late Triassic sediments in central Lhasa terrane, Tibet and its implication. *Gondwana Res.* **2014**, *25*, 1680–1689. [[CrossRef](#)]
88. Tang, S.-L.; Yan, D.-P.; Qiu, L.; Gao, J.-F.; Wang, C.-L. Partitioning of the Cretaceous Pan-Yangtze Basin in the central South China Block by exhumation of the Xuefeng Mountains during a transition from extensional to compressional tectonics? *Gondwana Res.* **2014**, *25*, 1644–1659. [[CrossRef](#)]
89. Veevers, J.; Saeed, A. Permian–Jurassic Mahanadi and Pranhita–Godavari Rifts of Gondwana India: Provenance from regional paleoslope and U-Pb/Hf analysis of detrital zircons. *Gondwana Res.* **2009**, *16*, 633–654. [[CrossRef](#)]
90. Myrow, P.M.; Hughes, N.C.; Paulsen, T.; Williams, I.; Parcha, S.K.; Thompson, K.; Bowring, S.A.; Peng, S.-C.; Ahluwalia, A. Integrated tectonostratigraphic analysis of the Himalaya and implications for its tectonic reconstruction. *Earth Planet. Sci. Lett.* **2003**, *212*, 433–441. [[CrossRef](#)]
91. Cawood, P.A.; Nemchin, A.A. Provenance record of a rift basin: U/Pb ages of detrital zircons from the Perth Basin, Western Australia. *Sediment. Geol.* **2000**, *134*, 209–234. [[CrossRef](#)]
92. Veevers, J.; Belousova, E.; Saeed, A.; Sircombe, K.; Cooper, A.; Read, S. Pan-Gondwanaland detrital zircons from Australia analysed for Hf-isotopes and trace elements reflect an ice-covered Antarctic provenance of 700–500 Ma age, TDM of 2.0–1.0 Ga, and alkaline affinity. *Earth-Sci. Rev.* **2006**, *76*, 135–174. [[CrossRef](#)]
93. Rangin, C.; Maw, W.; Lwin, S.; Naing, W.; Mouret, C.; Bertrand, G.; Party, G.S. Cenozoic pull-apart basins in central Myanmar: The trace of the path of India along the western margin of Sundaland. In Proceedings of the European Union of Geosciences conference, Strasbourg, France, 28 March–1 April 1999; p. 59.
94. Zhang, J.E.; Xiao, W.; Windley, B.F.; Wakabayashi, J.; Cai, F.; Sein, K.; Wu, H.; Naing, S. Multiple alternating forearc- and backarc-ward migration of magmatism in the Indo-Myanmar Orogenic Belt since the Jurassic: Documentation of the orogenic architecture of eastern Neotethys in SE Asia. *Earth-Sci. Rev.* **2018**, *185*, 704–731. [[CrossRef](#)]
95. Metcalfe, I. Tectonic framework and Phanerozoic evolution of Sundaland. *Gondwana Res.* **2011**, *19*, 3–21. [[CrossRef](#)]
96. Sun, S.-S.; McDonough, W.F. Chemical and isotopic systematics of oceanic basalts: Implications for mantle composition and processes. *Geol. Soc. Lond. Spec. Publ.* **1989**, *42*, 313–345. [[CrossRef](#)]
97. Stalder, M.; Rozendaal, A. *Trace and Rare Earth Element Chemistry of Garnet and Apatite as Discriminant for Broken Hill-Type Mineralization, Namaqua Province, South Africa*; Springer: Berlin/Heidelberg, Germany, 2005; pp. 699–702.

98. Nakada, R.; Shibuya, T.; Suzuki, K.; Takahashi, Y. Europium anomaly variation under low-temperature water-rock interaction: A new thermometer. *Geochem. Int.* **2017**, *55*, 822–832. [[CrossRef](#)]
99. Jafari, A.; Karimpour, M.H.; Mazaheri, S.A.; Malekzadeh Shafaroudi, A.; Ren, M. Geochemistry of metamorphic rocks and mineralization in the Golgohar iron ore deposit (No. 1), Sirjan, SE Iran: Implications for paleotectonic setting and ore genesis. *J. Geochem. Explor.* **2019**, *205*, 106330. [[CrossRef](#)]
100. Middelburg, J.J.; van der Weijden, C.H.; Woittiez, J.R. Chemical processes affecting the mobility of major, minor and trace elements during weathering of granitic rocks. *Chem. Geol.* **1988**, *68*, 253–273. [[CrossRef](#)]
101. Bhatia, M.R.; Crook, K.A. Trace element characteristics of graywackes and tectonic setting discrimination of sedimentary basins. *Contrib. Mineral. Petrol.* **1986**, *92*, 181–193. [[CrossRef](#)]
102. Brown, G.; Thorpe, R.; Webb, P. The geochemical characteristics of granitoids in contrasting arcs and comments on magma sources. *J. Geol. Soc.* **1984**, *141*, 413–426. [[CrossRef](#)]
103. Zhao, J.-H.; Zhou, M.-F.; Jian-Ping, Z. Metasomatic mantle source and crustal contamination for the formation of the Neoproterozoic mafic dike swarm in the northern Yangtze Block, South China. *Lithos* **2010**, *115*, 177–189. [[CrossRef](#)]
104. Saunders, A.; Storey, M.; Kent, R.; Norry, M. Consequences of plume-lithosphere interactions. *Geol. Soc. Lond. Spec. Publ.* **1992**, *68*, 41–60. [[CrossRef](#)]
105. Thompson, R.; Morrison, M. Asthenospheric and lower-lithospheric mantle contributions to continental extensional magmatism: An example from the British Tertiary Province. *Chem. Geol.* **1988**, *68*, 1–15. [[CrossRef](#)]
106. Mckenzie, D.; Bickle, M. The volume and composition of melt generated by extension of the lithosphere. *J. Petrol.* **1988**, *29*, 625–679. [[CrossRef](#)]
107. Rogers, N.; Macdonald, R.; Fitton, J.G.; George, R.; Smith, M.; Barreiro, B. Two mantle plumes beneath the East African rift system: Sr, Nd and Pb isotope evidence from Kenya Rift basalts. *Earth Planet. Sci. Lett.* **2000**, *176*, 387–400. [[CrossRef](#)]
108. Aung, W. Petrogenetic Studies of Metamorphic Rocks in Mogaung Area, Mogaung and Phakant Townships, Myitkyina District, Kachin State: Implication for Tectonic Setting. Ph.D. Thesis, University of Mandalay, Mandalay, Myanmar, 2008.
109. Gardiner, N.J.; Searle, M.P.; Morley, C.K.; Robb, L.J.; Whitehouse, M.J.; Roberts, N.M.; Kirkland, C.L.; Spencer, C.J. The crustal architecture of Myanmar imaged through zircon U-Pb, Lu-Hf and O isotopes: Tectonic and metallogenic implications. *Gondwana Res.* **2018**, *62*, 27–60. [[CrossRef](#)]
110. Li, S.; Yin, C.; Guilmette, C.; Ding, L.; Zhang, J. Birth and demise of the Bangong-Nujiang Tethyan Ocean: A review from the Gerze area of central Tibet. *Earth-Sci. Rev.* **2019**, *198*, 102907. [[CrossRef](#)]
111. Licht, A.; Win, Z.; Westerweel, J.; Cogné, N.; Morley, C.K.; Chantpraprasert, S.; Poblete, F.; Ugrai, T.; Nelson, B.; Aung, D.W. Magmatic history of central Myanmar and implications for the evolution of the Burma Terrane. *Gondwana Res.* **2020**, *87*, 303–319. [[CrossRef](#)]
112. Floyd, P.; Shail, R.; Leveridge, B.; Franke, W. Geochemistry and provenance of Rhenohercynian synorogenic sandstones: Implications for tectonic environment discrimination. *Geol. Soc. Lond. Spec. Publ.* **1991**, *57*, 173–188. [[CrossRef](#)]
113. Hennig, J.; Hall, R.; Armstrong, R.A. U-Pb zircon geochronology of rocks from west Central Sulawesi, Indonesia: Extension-related metamorphism and magmatism during the early stages of mountain building. *Gondwana Res.* **2016**, *32*, 41–63. [[CrossRef](#)]
114. Zimmermann, S.; Hall, R. Provenance of Mesozoic Sandstones in the Banda Arc Indonesia. In Proceedings of the 38 Annual Convention & Exhibition Indonesia, Indonesian Petroleum Association, Jakarta, Indonesia, 21–23 May 2014.
115. Zimmermann, S.; Hall, R. Provenance of Triassic and Jurassic sandstones in the Banda Arc: Petrography, heavy minerals and zircon geochronology. *Gondwana Res.* **2016**, *37*, 1–19. [[CrossRef](#)]
116. Fitzsimons, I. Grenville-age basement provinces in East Antarctica: Evidence for three separate collisional orogens. *Geology* **2000**, *28*, 879–882. [[CrossRef](#)]
117. Searle, M.P.; Whitehouse, M.J.; Robb, L.J.; Ghani, A.A.; Hutchison, C.S.; Sone, M.; Ng, S.W.-P.; Roselee, M.H.; Chung, S.-L.; Oliver, G.J.H. Tectonic evolution of the Sibumasu–Indochina terrane collision zone in Thailand and Malaysia: Constraints from new U-Pb zircon chronology of SE Asian tin granitoids. *J. Geol. Soc.* **2012**, *169*, 489–500. [[CrossRef](#)]
118. Stokes, R.B. A Review of Geology of Myanmar (Burma). Unpublished work. 1988.
119. UNDGSE. *Geology and Exploration Geochemistry of Part of the Northern and Southern Chin Hills and Arakan Yoma*; Western Burma, Technical Report No 4; UN/BUR-72-002/13; UNDP: Rangoon, Burma; UNDGSE: New York, NY, USA, 1979; 59p.
120. Bertrand, G.; Rangin, C.; Maluski, H.; Han, T.A.; Thein, M.; Myint, O.; Maw, W.; Lwin, S. Cenozoic metamorphism along the Shan Scarp (Myanmar): Evidences for ductile shear along the Sagaing Fault or the northward migration of the Eastern Himalayan Syntaxis? *Geophys. Res. Lett.* **1999**, *26*, 915–918. [[CrossRef](#)]